Global and Planetary Change 227 (2023) 104183

Contents lists available at ScienceDirect

Global and Planetary Change

journal homepage: www.elsevier.com/locate/gloplacha

Progressive marine oxygenation and climatic cooling at the height of the Great Ordovician Biodiversification Event

Nevin P. Kozik [a,*], Seth A. Young [a], Per Ahlberg [b], Anders Lindskog [a,b], Jeremy D. Owens [a]

[a] Department of Earth, Ocean, and Atmospheric Science and National High Magnetic Field Laboratory, Florida State University, Tallahassee, FL 32306, USA
[b] Department of Geology, Lund University, Sölvegatan 12, SE-223 62 Lund, Sweden

ARTICLE INFO

Editor: Dr. Maoyan Zhu

Keywords:
Middle Ordovician
Thallium isotopes
Sulfur isotopes
Marine biodiversity
Trace metals
Paleoredox

ABSTRACT

The oxygen content of ancient seawater has been hypothesized to be a major controlling factor for biodiversity throughout Earth's history. The Great Ordovician Biodiversification Event (GOBE) represents one of the largest increases in biodiversity during the Phanerozoic, with peak rates of diversity occurring in the Middle–Late Ordovician. Multiple causal factors have resulted in this long-term adaptive radiation, but direct links to marine oxygen levels remain poorly characterized. Here we utilize a multiproxy dataset from the Röstånga-2 drillcore, Skåne (Scania), southernmost Sweden, to constrain local and global marine paleoredox dynamics using a multiproxy approach throughout the Middle–Late Ordovician (Darriwilian–early Sandbian stages). Pyrite sulfur isotopes ($\delta^{34}S_{pyr}$), iron speciation and trace metal concentrations (V, U, and Mo) all indicate pervasive locally reducing conditions, and thallium ($\varepsilon^{205}Tl$) isotopic compositions indicate significant changes in global Mn-oxide burial. This is one of the first studies to utilize direct local and global paleoredox proxies to identify changes in marine oxygen associated with peak rates of biodiversification in the Ordovician. Our new thallium isotope and pyrite sulfur isotope trends from black shale are combined with previously published carbonate-based redox proxy data ($\delta^{238}U$ and $\delta^{34}S_{CAS}$–carbonate-associated sulfate) from time equivalent successions in Baltica, Laurentia and Argentine Precordillera, indicating a global shift towards enhanced Mn-oxide burial, decreased anoxic seafloor area, and decreased pyrite burial, respectively. Thus, oceanic conditions during the Middle–Late Ordovician are interpreted to have transitioned from pervasive, highly reducing conditions towards more oxygenated marine settings. These changes in global paleoredox coincide with paleotemperature proxy data that indicated an overall climatic cooling trend during this time. Significant cooling of Ordovician oceans and climate would have permitted enhanced ventilation of marine environments, that in turn likely facilitated new ecospace development/utilization and ultimately drove marine biodiversification. Our results show a protracted, yet progressive oxygenation of marine environments over an interval of ~11 Myr coinciding with peak rates of biodiversification during the GOBE.

1. Introduction

The Ordovician Period (~485–445 Ma) hosted one of the largest intervals of marine biodiversification, commonly referred to as the Great Ordovician Biodiversification Event (GOBE) or the Ordovician Radiation, which accommodated an unprecedented increase in faunal richness among marine taxonomic groups that were established during the Cambrian Explosion (Sepkoski et al., 1981; Harper, 2006; Rasmussen et al., 2019). This proliferation of marine faunas was subsequently terminated by the second-largest mass extinction in Earth history, the Late Ordovician Mass Extinction Event (LOME; Harper, 2006; Harper et al., 2014). While recent studies documenting biodiversity trends have greatly advanced our understanding of the potentially nuanced changes in ecospace, the definition and timing (and internal nomenclature) of the GOBE is still widely debated (Rasmussen et al., 2019; Stigall et al., 2019; Servais et al., 2021; Deng et al., 2021). There is currently no clear consensus as to when the GOBE started due to highly variable resolution among datasets and preservation biases; however, most studies have identified "peak" faunal richness within the Dapingian–Sandbian stages. Additionally, primary causal mechanisms for the GOBE remain uncertain, although dynamic fluctuations in paleoredox conditions have been identified and proposed as a contributing factor (Kah et al., 2016; Young

* Corresponding author.
E-mail address: nkozik@fsu.edu (N.P. Kozik).

https://doi.org/10.1016/j.gloplacha.2023.104183
Received 3 March 2023; Received in revised form 8 June 2023; Accepted 23 June 2023
Available online 25 June 2023

et al., 2016; Edwards et al., 2017; Edwards, 2019; Rasmussen et al., 2019; Stigall et al., 2019). Currently, there are a multitude of studies that have focused on paleoredox conditions surrounding the LOME and a growing number focusing on redox dynamics associated with the GOBE (i.e., the Early–Middle Ordovician) (e.g., Harper, 2006; Harper et al., 2014; Rasmussen et al., 2019; Stigall et al., 2019). Despite these efforts, the causal mechanisms for changing paleoenvironmental conditions and the evolutionary radiation in the Ordovician – especially those surrounding the peak of biodiversification during the Middle Ordovician – are not well understood, and thus the impact of these processes on global marine biodiversity remains under-constrained.

Geochemical studies have shown strong links between increased oxygenation and the rise of metazoan life (Fike et al., 2006; Kendall et al., 2015; Sahoo et al., 2016; Ostrander et al., 2020); however, the link (s) between biodiversification of already established ecosystems and fluctuating oxygenation needs further investigation (Elmqvist et al., 2003; Sampaio et al., 2021). Several studies have attempted to quantify changes in atmospheric and marine oxygenation throughout the Ordovician. These studies primarily utilize traditional proxies such as $\delta^{13}C$ and $\delta^{34}S$ but ultimately disagree in terms of the magnitude of change in oxygenation. Nonetheless, many of these studies generally find that elevated oxygen levels coincide with biodiversity pulses identified as part of the GOBE (Sperling et al., 2015; Edwards et al., 2017; Krause et al., 2018; Lenton et al., 2018). Currently, very few studies have utilized direct and multiple paleoredox proxies and combined geochemical proxies from multiple lithologies through this interval of biodiversification, and thus the role of enhanced oxygenation as a causal mechanism for the interval of peak diversity remains uncertain. An overall increase in well-oxygenated conditions subsequently would have allowed for enhanced heterotrophic metabolic processes, that might fuel increased predation as well as adaptations to avoid this predation, allowing for flourishing seascapes that harbored more diverse and varied marine ecosystems. Currently, some studies that have utilized carbonate-associated sulfate isotopic compositions (CAS; $\delta^{34}S_{CAS}$) have identified a potential global reduction in pyrite burial, which may indicate a reduction in the total extent of highly reducing euxinic (euxinic = anoxic + sulfidic) conditions (Thompson and Kah, 2012; Kah et al., 2016; Young et al., 2016; Edwards et al., 2019). These studies have primarily been performed in carbonate-dominated successions, predominantly on the Laurentian, and South China paleocontinents and in the Argentine Precordillera. Meanwhile, even fewer studies have utilized deeper-water, organic-matter rich shales to elucidate changes associated with this biotic event in the Ordovician (e.g., Sperling et al., 2021; Zhang et al., 2022). In this study, we present a multiproxy dataset from an organic-matter rich shale-dominated sequence that spans the Middle to lower Upper Ordovician (Darriwilian to early Sandbian stages) from the paleocontinent of Baltica, to examine changes in marine oxygenation and its potential relationship to the peak diversification rates of the GOBE.

2. Background

The Röstånga-2 drill core is comprised of a relatively thick and mostly complete sequence of Middle to Late Ordovician organic-matter rich shales that originates from west-central Skåne (Scania), southern Sweden. The Röstånga-2 drill core is one of several cores spanning the Middle–Upper Ordovician of Skåne. Other drill cores that originate from this area include the Krapperup, Lerhamn, and Röstånga-1 cores, and the Fågelsång-1, -2, and -3 cores (Bergström et al., 1999, 2014, 2018; Maletz and Ahlberg, 2011, 2021; Maletz et al., 2020) . This study will focus primarily on the Almelund and Sularp Shale formations (Bergström et al., 2002) within the Röstånga-2 drill core, which has been the subject of lithologic, graptolite biostratigraphic and carbon isotopic studies (Bergström et al., 2020; Maletz et al., 2020); the succession is confidently placed within the Middle to Upper Ordovician (Dw2 through Sa1 stage slices; Bergström et al., 2009). Here, we utilize bulk stable organic carbon isotopic compositions previously published by Bergström et al. (2020) as well as established detailed graptolite biostratigraphy by Maletz et al. (2020) for our chronostratigraphic framework. The Röstånga-2 drill core is interpreted to reflect deposition in an outer shelf–upper slope setting on the western margin of the paleocontinent of Baltica, at ~45°S paleolatitude (Fig. 1; Torsvik et al., 2012; Lindskog and Eriksson, 2017). Lithologically, the Röstånga-2 drill core is composed entirely of finely laminated dark grey to black shales, with a minor phosphatic-rich interval (Fågelsång phosphorite bed) in the upper part of the core (Fig. 2). The Almelund and Sularp shales differ in litho- and biofacies from coeval successions in other areas of Sweden and the East Baltic area, in which the pre-Katian Ordovician is dominated by shallower-water carbonates that were deposited on the cratonic interior. The black shale interval below the Fågelsång phosphorite bed are within the Almelund Shale Formation, and the black shales above this horizon are within the Sularp Shale Formation (Fig. 2; Bergström et al., 2020).

2.1. Pyrite sulfur isotopes

The oxidation and reduction of sulfur has played a role in modulating atmospheric composition throughout Earth history via biotic and abiotic processes (Fike et al., 2015; Canfield, 2019). The sulfur cycle starts with the weathering of sulfide minerals on the continental crust as well as volcanic outgassing providing an input of sulfate (SO_4^{2-}) into marine settings. If redox conditions are sufficiently reducing, microbial sulfate reduction (MSR) couples the carbon and sulfur cycles through the oxidation of marine organic matter and using sulfate as an electron acceptor which in turn produces hydrogen sulfide as a byproduct that can react with aqueous Fe^{2+} to ultimately form pyrite (FeS_2) on geologic timescales (Canfield et al., 1992). Pyrite sulfur isotopes ($\delta^{34}S_{pyr}$) have the potential to reflect trends in either local or global MSR rates, however, several aspects of the sulfur cycle must be constrained for global interpretations. These aspects include the location of MSR (either in the sediments or in the water column, i.e., open or closed system pyrite formation), marine sulfate concentrations and the magnitude of the kinetic isotopic effects (Gomes and Hurtgen, 2015; Lang et al., 2020; Pasquier et al., 2021).

2.2. Iron geochemistry

Iron geochemistry from organic-rich shales is a well-used paleoredox proxy in constraining local redox conditions through the ratios of various Fe phases. Within reducing marine settings, higher contents of "highly reactive" iron are present in the form of pyrite, siderite, and other crystalline Fe-oxyhydroxides (i.e., ferrihydrite, lepidocrocite, goethite, hematite). Thus, the ratio between highly reactive iron (Fe_{HR}) to total iron (Fe_T) informs about local paleoredox conditions within the depositional basin (Poulton and Canfield, 2005; Raiswell et al., 2018). Ratios of Fe_{HR}/Fe_T higher than 0.38 have been shown to be deposited under anoxic conditions, whereas values between 0.22 and 0.38 may have complications that mask the enrichment of highly reactive iron such as high sedimentation rates. If sediments are interpreted to have been deposited under anoxic conditions, ratios between pyrite iron (Fe_{pyr}) and Fe_{HR} is used to determine if the anoxic conditions were ferruginous (anoxic and Fe^{2+} rich, or sulfate limited) or euxinic (anoxic and sulfide-rich, or iron-limited). Values of Fe_{pyr}/Fe_{HR} above 0.70 are likely to have been deposited under euxinic conditions, whereas values below this were deposited under ferruginous conditions.

2.3. Trace metal geochemistry

The concentrations of several trace metals within sedimentary rocks have been used to infer changes in both local and global redox throughout geologic history (Algeo and Lyons, 2006; Anbar et al., 2007; Scott and Lyons, 2012; Reinhard et al., 2013). The concentrations of trace metals discussed below are primarily controlled by local redox

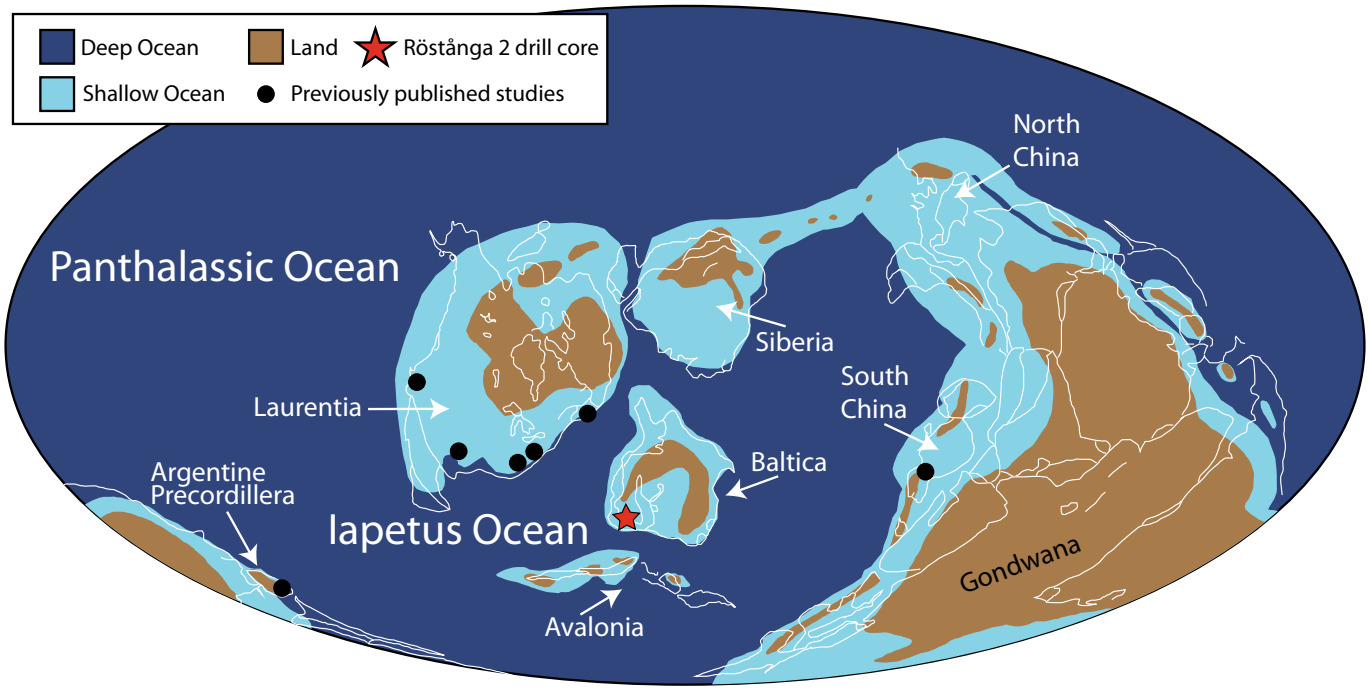

Fig. 1. Paleogeographic reconstruction of the Middle Ordovician world (modified from Scotese, 2001), with the approximate location of the Röstånga-2 drill core indicated as a red star. Other paleoredox studies are shown as black circles. (For interpretation of the references to colour in this figure legend, the reader is referred to the web version of this article.)

conditions. However, trace metal dynamics may also reflect changes within an individual element's global marine reservoir, ultimately hinting at global redox conditions, if persistent local anoxia/euxinia is identified utilizing independent proxies such as iron speciation. In this study, we focus on the elemental cycles of manganese (Mn), vanadium (V), uranium (U), and molybdenum (Mo), each of which have differing reduction potentials, and thus have slightly different responses to changes in local and global marine redox.

Due to the element's rapid response to reducing conditions and its very short residence time of ~0.06 kyr, Mn concentrations are commonly used as a local redox proxy (Froelich et al., 1979; Maynard and Force, 1991; Tribovillard et al., 2006). Under slightly reducing conditions, solid Mn-oxides ($Mn^{3+/4+}$) are quickly reduced to aqueous Mn^{2+} due to the high redox potential (Froelich et al., 1979; Rue et al., 1997; Algeo and Maynard, 2008). Aqueous Mn^{2+} can then either be recycled into the overlying water column or associated with Mn-bearing minerals such as sulfides and carbonates (Maynard and Force, 1991; Calvert and Pedersen, 1996; Algeo and Maynard, 2008). Concentrations less than the average oxic shale values of 850 ppm generally indicate deposition under reducing conditions, while concentrations above this threshold are generally associated with oxidizing conditions (Taylor and McLennan, 1981, 1995; Maynard and Force, 1991). Mn oxide burial fluxes also influence Tl isotopic compositions (Owens, 2019); thus Tl isotopes can be used to fingerprint the global Mn oxide flux, which can be related back to changes in global bottom-water oxygenation states (see Section 2.4 for further explanation).

Unlike manganese, V has a longer residence time of ~50 to 100 kyr. Within oxic waters, vanadium forms aqueous and stable HVO_4^{2-} and $H_2VO_4^-$ ions (with V(V) oxidation state) that behave mostly conservatively, but can adsorb to Mn and Fe-oxides (Tribovillard et al., 2006). However, under mildly reducing conditions, V(V) is reduced to V(IV), which forms insoluble $VO(OH)_2$ and $VO(OH)_3^-$, which can complex with humic acids and ultimately be buried within sediments. Under euxinic conditions, V(IV) can be further reduced to V(III) and be precipitated into solid V_2O_3 or V-oxyhydroxides (Tribovillard et al., 2006). With the initial reduction of V under low oxygen conditions, enrichment is not dependent on the presence of sulfide and thus has been used to indicate changes in global anoxia (Hetzel et al., 2009; Owens et al., 2016; Young et al., 2020).

Uranium has the longest residence time of all the elements that are discussed in this study, with a residence time of ~450 kyr. The sedimentary concentration of U is dependent on the redox state, as the dominant species of U is soluble U(VI) and generally bound to carbonate ions to form $UO_2(CO_3)_3^{4-}$. Under mildly reducing conditions, similar to that of Fe reduction, U(VI) is reduced to insoluble U(IV) species such as UO_2 (Lau et al., 2019; Owens, 2019). Oxygen penetration depths and sedimentation rates are important aspects to consider for the evaluation of authigenic U enrichments, as U reduction is thought to occur primarily in the sediments, decoupled from early redox responses (i.e., O_2, NO_3^- and/or Mn reduction) and MSR. Thus, slow sedimentation rates allow more time for oxidized species to diffuse into sediments, resulting in erroneously high enrichments (Tribovillard et al., 2006). Conversely, U is easily re-oxidized, wherein authigenic U can be removed if O_2 penetration depths encroach into the Fe reduction chemocline, resulting in erroneously low enrichments (McManus et al., 2005).

Molybdenum has a relatively long residence time of ~440 kyr and is the most abundant transition metal in modern oceans (Tribovillard et al., 2006). Similarly to vanadium, Mo forms stable molybdate (MoO_4^{2-}) ions under oxic conditions which can adsorb onto Mn and Fe-oxides (Algeo and Tribovillard, 2009), which produces sedimentary concentrations similar to crustal values of ~2 ppm (Taylor and McLennan, 1995). In the presence of H_2S, Mo is efficiently enriched within sediments through the reduction of molybdate into thiomolybdates (MoO_xS_{4-x}, where x = 0 to 3) which are particle reactive and prone to scavenging by sulfides and sulfur rich organic molecules (Erickson and Helz, 2000). Mild enrichments entail concentrations between 25 and 100 ppm of Mo and likely indicate deposition in the presence of sulfidic porewaters or true euxinia within the water column. Meanwhile Mo concentrations between 2 and 25 ppm likely indicates deposition under either intermittently euxinic/sulfidic conditions, dilution via high sedimentation rates, variability in water column pH, or most importantly changes in dissolved concentrations within the water

column or global marine inventory (Scott and Lyons, 2012; Hardisty et al., 2018). Lastly, highly enriched sediments, with concentrations larger than 100 ppm of Mo, are considered a strong indicator of water column euxinia with little to no complications in the dissolved concentrations of Mo or connection to open marine conditions (Scott and Lyons, 2012; Hardisty et al., 2018).

The use of enrichment factors is a common tool to compare the authigenic enrichment of given redox sensitive trace metals with varying upper continental crustal concentrations, by normalizing a given trace metal to detrital aluminum. Here we employ the use of enrichment factors, following the convention of Algeo & Tribovillard, (2009); $X_{EF} = [(X/Al)_{sample}/(X/Al)_{PAAS}]$, where X stands for the concentration of a given redox sensitive metal and Al stands for the concentration of aluminum. Sample concentrations are then normalized to the composition of post-Archean average shale, or PAAS (Taylor and McLennan, 1995). Enrichment factors ≈ 1 are considered to represent no enrichment, but rather values equal to background sedimentation, while enrichment factor values ≥3 are generally considered to be noticeable, and lastly, enrichments ≥10 are considered substantial (Algeo and Tribovillard, 2009).

2.4. Thallium isotopes

Sedimentary Tl isotopic compositions are an emerging paleoredox proxy that has been utilized to elucidate changes in global Mn-oxide burial flux (Ostrander et al., 2017, 2019, 2020; Them et al., 2018; Bowman et al., 2019; Fan et al., 2020; Newby et al., 2021). Tl isotopic compositions (reported as $\varepsilon^{205}Tl = ({}^{205/203}Tl_{sample} - {}^{205/203}Tl_{NIST\text{-}997})/{}^{205/203}Tl_{NIST\text{-}997} \times 10^4$) of modern seawater are homogenous ($\varepsilon^{205}Tl_{seawater} = -6 \pm 0.3$), reflecting its long residence time of ~18.5 kyr compared to ocean mixing of ~1–2 kyr (Owens et al., 2017; Owens, 2019). The Tl isotopic mass balance has been well established and shows that changes in marine isotopic compositions are primarily controlled by the relative strengths of output fluxes, the alteration of oceanic crust (AOC) ($\varepsilon^{205}Tl_{AOC} = -12$ to -6) and burial of Mn-oxides ($\varepsilon^{205}Tl_{Mn\text{-}oxides} = +6$ to $+12$), as most inputs of Tl are isotopically similar ($\varepsilon^{205}Tl_{inputs} = \sim -2$; Nielsen et al., 2011; Owens et al., 2017). Importantly, changes in the burial rate of Mn-oxides have the largest isotopic difference between seawater and output flux, as well as occurring on short timescales (in a geologic perspective, i.e., less than multi–million–year process). Seawater values are obtained via adsorption to authigenic pyrite precipitation in anoxic or euxinic settings, and is not thought to produce any isotopic fractionation (Owens et al., 2017).

3. Materials and Methods

3.1. Sample collection and preparation

The Röstånga-2 core is housed at the Department of Geology, Lund University, Sweden, where sampling and detailed lithologic descriptions were undertaken. Samples for geochemical analyses were collected at ~50 cm intervals to be conducted at Florida State University (FSU) and the National High Magnetic Field Laboratory (NHMFL-FSU), Tallahassee, USA. This sample spacing results in a resolution of approximately two samples per million years (see Section 5.2 for further details). Samples were selected from horizons that contain no obvious secondary recrystallization of sulfate or carbonate minerals, calcite veins, secondary pyrite nodules or from brecciated strata associated with nearby faulting. Samples were cleaned in an ultrasonic bath of deionized water (18.2 MΩ) to remove weathered surfaces and/or drilling mud residue, then dried and powdered using an agate mortar and pestle. Splits of each powdered sample were utilized for the geochemical analyses discussed below.

3.2. Organic carbon isotopes

A total of 30 samples from the Röstånga-2 core were analyzed for total organic carbon (TOC). Approximately 0.5 g of powdered sample were weighed into clean centrifuge tubes and reacted with 6 N HCl to remove the minor carbonate component throughout the core. Samples were acidified then rinsed with deionized water (18.2 MΩ) three times each and left to dry in an oven at 70 °C overnight. Residues were then homogenized and weighed into tin cups for isotopic analysis. Organic carbon isotopic analysis was performed using a Carlo Erba Elemental Analyzer coupled to a ThermoFinnegan Delta Plus XP isotope ratio mass spectrometer (IRMS) via a Conflo-III device. Sample precision and calibration of data were assessed during routine analysis of laboratory standards that are calibrated against IAEA standards, and are reported in wt% TOC. Carbon standards at NHMFL-FSU include Acetanilide, Urea-2, and WYSTD. Weight percent of total organic carbon in samples is determined by comparison to voltages for the CO_2^+ ion beam intensities for masses 44, 45 and 46 between unknowns and known wt% of carbon of the gravimetric standard Acetanilide analyzed during the same sequence. The uncertainty of these TOC measurements is better than ±5%.

3.3. Pyrite sulfur extraction

The same samples analyzed for TOC were prepared for sedimentary pyrite extractions following a modified chromium reducible sulfur extraction procedure from Brüchert and Pratt (1996). Powdered samples (~0.5–2.0 g) were weighed into glass extraction flasks, where powders were reacted with a mixture of 70 ml of 12 M HCl and 30 ml of 1.0 M of $CrCl_2$ that was continuously heated and agitated for 2–3 h. Evolved H_2S gas was passed through a mixture of 0.1 M sodium citrate buffered to a pH of 4, then passed through a 0.1 M $AgNO_3$ solution to precipitate Ag_2S. The Ag_2S was filtered, rinsed (with 18.2 MΩ deionized water), dried and weighed for concentration determinations. Total weight of Ag_2S precipitate were gravimetrically determined to calculate wt% pyrite assuming the quantitative conversion and stoichiometry of Fe_2S into Ag_2S, and subsequently used to calculate pyrite Fe (Fe_{pyr}, see more in Section 3.4). Pyrite sulfur isotopic analysis was measured using a Thermo-Isolink Elemental Analyzer coupled to a Thermo Delta V Plus IRMS via a Dual Inlet system. Sample precision and calibration of data was determined during routine analysis of laboratory standards that were calibrated against IAEA standards and reported in standard delta-notation (δ) with units reported in per mill (‰) relative to VCDT (Vienna Canyon Diablo Troilite). Sulfur isotope standards at the NHMFL-FSU include IAE 3 S-3 (−32.3‰), PQM2 (−16.0‰), ERE Ag_2S (−4.7‰), EMR-CP (0.9‰), SWP (20.7‰), and PQB-D (40.5‰). Analytical precision for $\delta^{34}S_{pyr}$ is ±0.2‰ or better.

3.4. Iron speciation

The same 30 samples selected for pyrite isotope analysis were analyzed for sequential Fe extractions (henceforth Fe speciation), following procedures outlined by Poulton and Canfield (2005). Approximately 0.1 g of powdered samples were weighed into clean 15 ml centrifuge tubes. The first extraction used 10 ml of 1.0 M sodium acetate, buffered to pH 4.5 and allowed to react with samples for 24 h to extract Fe from carbonate minerals (Fe_{carb}). Second, 10 ml of 0.29 M sodium dithionite buffered to pH 4.8 with 0.35 acetic acid and sodium citrate was allowed to react with samples for 2 h to extract Fe from oxides and oxyhydroxides (Fe_{ox}). Lastly, 0.2 M ammonium oxalate and 0.17 M oxalic acid buffered to pH 3.2 with ammonium hydroxide were allowed to react with samples for 6 h to extract Fe from magnetite (Fe_{mag}). Following each step, samples were centrifuged, and supernatant was saved for analysis. Each sample was rinsed with 18.2 MΩ deionized water, centrifuged and decanted before each extraction. The supernatant from each extraction was diluted with 2% ultrapure HNO_3 and

analyzed for Fe concentrations using an Agilent 7500cs inductively-coupled plasma mass spectrometer (ICP-MS) at the NHFML-FSU. Highly reactive Fe (Fe_{HR}) was calculated from the sum of all species: $Fe_{carb} + Fe_{ox} + Fe_{mag} + Fe_{pyr}$. Duplicate samples had reproducibility of ±7% for the entire extraction method.

3.5. Trace metal concentrations

Trace metal concentration was analyzed for the same samples selected for iron speciation and pyrite isotope analysis, through multi-acid digestion. Samples were weighed (~100 mg) into Savillex beakers and underwent microwave digestion using a CEM MARS 6 to digest organic carbon. Samples were then dissolved completely using subsequent treatment of trace metal free HNO_3, HCl, and HF. Acids were allowed to react with samples with heat (~120–180 °C) for 24–48 h and dried down completely before adding different and additional acids. Following complete dissolution of sample powder, samples were dried down and dissolved into 2% HNO_3 and analyzed on an Agilent 7500cs ICP-MS (at NHFML-FSU) for trace metal concentration. Samples were compared to USGS standards SDO-1, SCO-1 and SGR-1 that were dissolved alongside samples and were all within accepted analytical ranges for all analyzed elements. All results are reported as parts per million (ppm) with a precision of ±5% or better for Mo, V, Fe, and Mn. A common tool to compare the authigenic enrichments of trace metals with differing redox responses as well as differing background concentrations (i.e., UCC concentrations) is the normalization to detrital aluminum in the form of enrichment factors (Algeo and Tribovillard, 2009). We present the enrichment factors (EF) for several trace metals calculated as: $X_{EF} = [(X/Al)_{sample}/(X/Al)_{PAAS}]$, where X stands for the concentration of a given redox sensitive metal and Al stands for the concentration of aluminum within a given sample. Sample concentrations are then normalized to the composition of post-Archean average shale, or PAAS (Taylor and McLennan, 1995). Generally, enrichment factors above 3 are considered to reflect noticeable enrichment above background sedimentation, and enrichments above 10 are considered substantial (Algeo and Tribovillard, 2009).

3.6. Thallium isotopes

A subset (28 total) of the samples analyzed for TOC, iron speciation and trace metal concentrations were analyzed for thallium isotopes following a modified procedure outlined by Nielsen et al. (2011) and Owens et al. (2017). Briefly, samples that were chosen for trace metal analysis were weighed (100 mg) into clean Savillex beakers and allowed to react with 2 M HNO_3 at 130 °C for 12 h to separate leachable Tl adsorbed to pyrite. The supernatant from the leaching was then purified of Pb using micro-columns filled with Bio-Rad AG1-X8 resin following established column chemistry procedures (Nielsen et al., 2011; Owens et al., 2017). Samples were subsequently analyzed for Tl concentration using an Agilent 7500cs ICP-MS, then spiked with NIST-SRM-981 Pb to track mass bias during mass spectrometry analysis (Nielsen et al., 2005). Tl isotopes were analyzed with a Neptune multicollector (MC) ICP-MS using an Aridus II autosampler at the NHMFL-FSU. All Tl isotopes are reported as ε^{205}Tl. Long term precision was determined using USGS SCO-1 reference material with $\varepsilon^{205}T = -3.00 \pm 0.3$ (2σ). Samples reported here have an uncertainty of less than ±0.5 (2σ, based on two or more replicate analyses), however any samples with uncertainty less than ±0.3 were subsequently increased to ±0.3 based on the error for the geostandard from the entire method.

4. Results

High-resolution carbon isotope data for the Röstånga-2 core has previously been published, which potentially document the Middle Darriwilian Isotope Carbon Excursion (MDICE) in the *Pterograptus elegans* and *Pseudamplexograptus distichus* graptolite biozones (Bergström et al., 2020). Our new $\delta^{34}S_{pyr}$ dataset identifies two long term trends, with the first shift occurring within the *Holmograptus lentus* graptolite Biozone, and the second occurring within the *Pt. elegans* Biozone (Fig. 2). The first and earlier trend of $\delta^{34}S_{pyr}$ values shifting more positively, albeit with fluctuations, from approximately −20‰ in the *H. lentus* Biozone to values averaging at approximately −0.5‰, with maximum values of +6‰ in the lower *Pt. elegans* Biozone. Subsequently $\delta^{34}S_{pyr}$ values decline sharply within the middle *Pt. elegans* Biozone to ~ −15‰ in the middle and upper part of the MDICE interval. Lastly, $\delta^{34}S_{pyr}$ values continue to decline to values between −29‰ to −20‰ within the *Nemagraptus gracilis* graptolite Biozone.

Our iron speciation (Fe_{HR}/Fe_T) indicates an array of values, mostly falling within the possibly anoxic range (between 0.20 and 0.38) with few values falling in both the oxic and anoxic range. On the other hand, all but seven Fe_{pyr}/Fe_{HR} values fall above the euxinic threshold of 0.8. Our trace metal concentrations show moderate enrichments of nearly all typically reported redox sensitive metals such as V, U and Mo. Trends in Mo show concentration range between ~5 ppm and ~ 18 ppm, with some minor cyclical fluctuations with a ~ 40-m frequency. Enrichment factors for Mo (Mo_{EF}) show nearly identical trends as concentrations

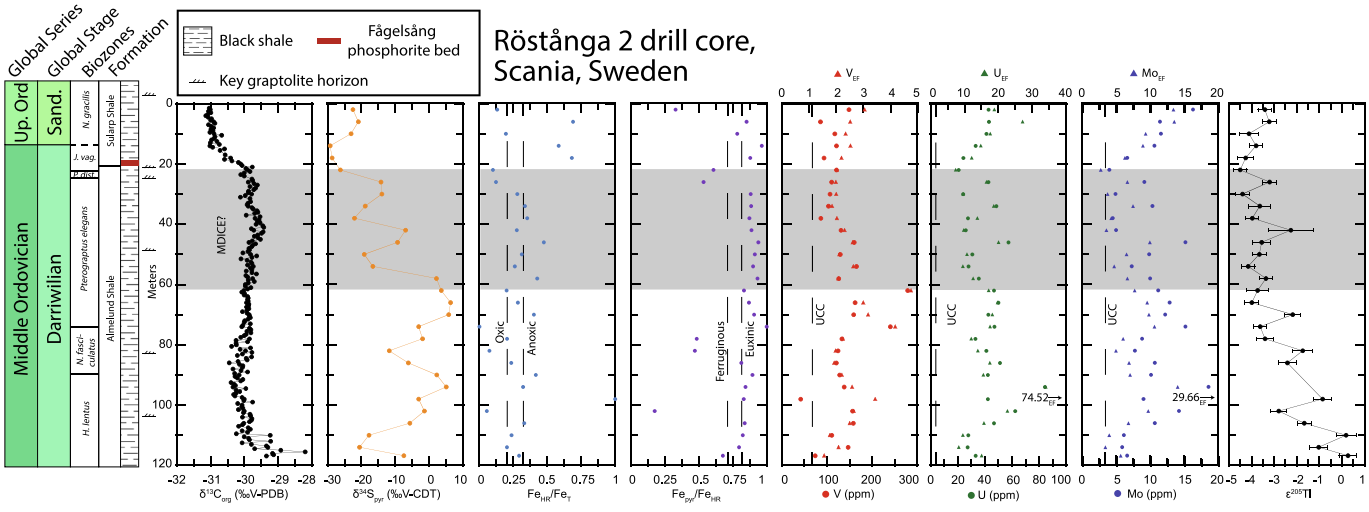

Fig. 2. Middle–Upper Ordovician geochemical profiles of the Röstånga-2 drill core. Graptolite biostratigraphy, lithostratigraphy and $\delta^{13}C_{org}$ data are replotted from previous studies (Bergström et al., 2020; Maletz et al., 2020). The grey bar indicates the MDICE interval. UCC = upper continental crust. *P. dist.* = *Pseudamplexograptus distichus*; *J. vag.* = *Jiangxigraptus vagus*.

apart from of a couple of datapoints within the *H. lentus* Biozone, where Mo_{EF} is significantly greater than concentrations. In the Röstånga-2 drill core, all Mo_{EF} values are ≥3 and several intervals exceed values of 10, particularly within the *H. lentus* and *N. gracilis* biozones. Similar to that of Mo, V and U show mild enrichments, with concentrations ranging between ~40 ppm and ~ 280 ppm for V whereas U concentrations range between ~20 ppm and ~ 85 ppm. Enrichment factors for both elements show nearly identical trends, apart from the same interval within the *H. lentus* Biozone, in which some datapoints show inverse trends. Both V and U show the same cyclical fluctuations as Mo in both concentrations as well as enrichment factors. Combined enrichment factors for all of these trace metals indicate at least sulfidic porewaters to potentially euxinic bottom water conditions, given the additional complications such as geochemical dilution due to high sedimentation rates. Lastly, our Tl isotopic dataset shows a progressive negative trend from maximum values of $\varepsilon^{205}Tl$ of ~ −1 in the lower *H. lentus* Biozone at the base of the drill core to minimum values of $\varepsilon^{205}Tl = \sim -4.5$ in the *Pt. elegans* and *Jiangxigraptus vagus* biozones.

5. Discussion

The use of geochemical cross plots is a common tool that can be used to assess the preservation of primary geochemical signatures for the Röstånga-2 drill core (Fig. 3). The lack of a well correlated relationship (i.e., high R^2 value) between $\delta^{13}C_{org}$ and TOC wt% indicates minimal thermal heating and oxidation-related loss of organic compounds (Meyers, 1994; Hayes et al., 1999). Similarly, the weakly correlated trend between $\delta^{34}S_{pyr}$ and pyrite concentrations (ppm) suggests little to no oxidative loss of pyrite resulting from late diagenetic processes. The weak to nonexistent relationships between the Mn, V, U and Al wt% may indicate only minor late diagenetic influence due to metal incorporation into silicate fractions (Fig. 3C, D). Our cross plots also show a weak or no relationship between our Tl isotopic compositions, Mn, and Tl concentrations, indicating that the Tl isotopic compositions likely reflect primary seawater. Ultimately, our cross plots show weak to no correlation between various geochemical datasets, likely indicating the preservation of mostly primary paleoredox signatures.

Lastly, we identify nearly synchronous first-order changes in $\delta^{34}S_{pyr}$ within the Röstånga-2 drill core, similar to other sulfur isotope records ($\delta^{34}S_{CAS}$) from carbonate successions in Laurentia, Argentine Precordillera and South China (Thompson and Kah, 2012; Kah et al., 2016; Young et al., 2016; Edwards et al., 2019). This drop in $\delta^{34}S_{pyr}$, which begins within the lowest portion of the *Pt. elegans* graptolite Biozone, preceeds the initial drop in $\delta^{34}S_{CAS}$ records, which primarily record a major decline within the uppermost portion of the *E. pseudoplanus* to lowermost portion of the *E. suecicus* conodont biozones (Fig. 4). Due to the shale-dominated lithology of this drill core, we are unable to produce a coeval $\delta^{34}S_{CAS}$ dataset alongside our new $\delta^{34}S_{pyr}$ dataset that would allow for a more direct integration of the two sulfur isotopic records. Changes in authigenic $\delta^{34}S_{pyr}$ are generally thought to reflect changes in local sulfur cycling and possibly early stage diagenetic processes. However, given the very different lithologies and tectonic development between our site in Baltica compared to other marine basins with $\delta^{34}S_{CAS}$ records, it is very unlikely that the Röstånga-2 drill core experienced similar diagenetic histories to those found on western and eastern Laurentia, Argentine Precordillera and South China during this time. Given that pyrite sulfur isotopic compositions can be influenced by a variety of local factors that range from sedimentation rate, local oxygen penetration depths and type of organic matter that is produced in each basin (e.g., Gomes and Hurtgen, 2015), it is unlikely these disparate basins would each have similar depositional and post-depositional histories given the differences in lithologies, relative

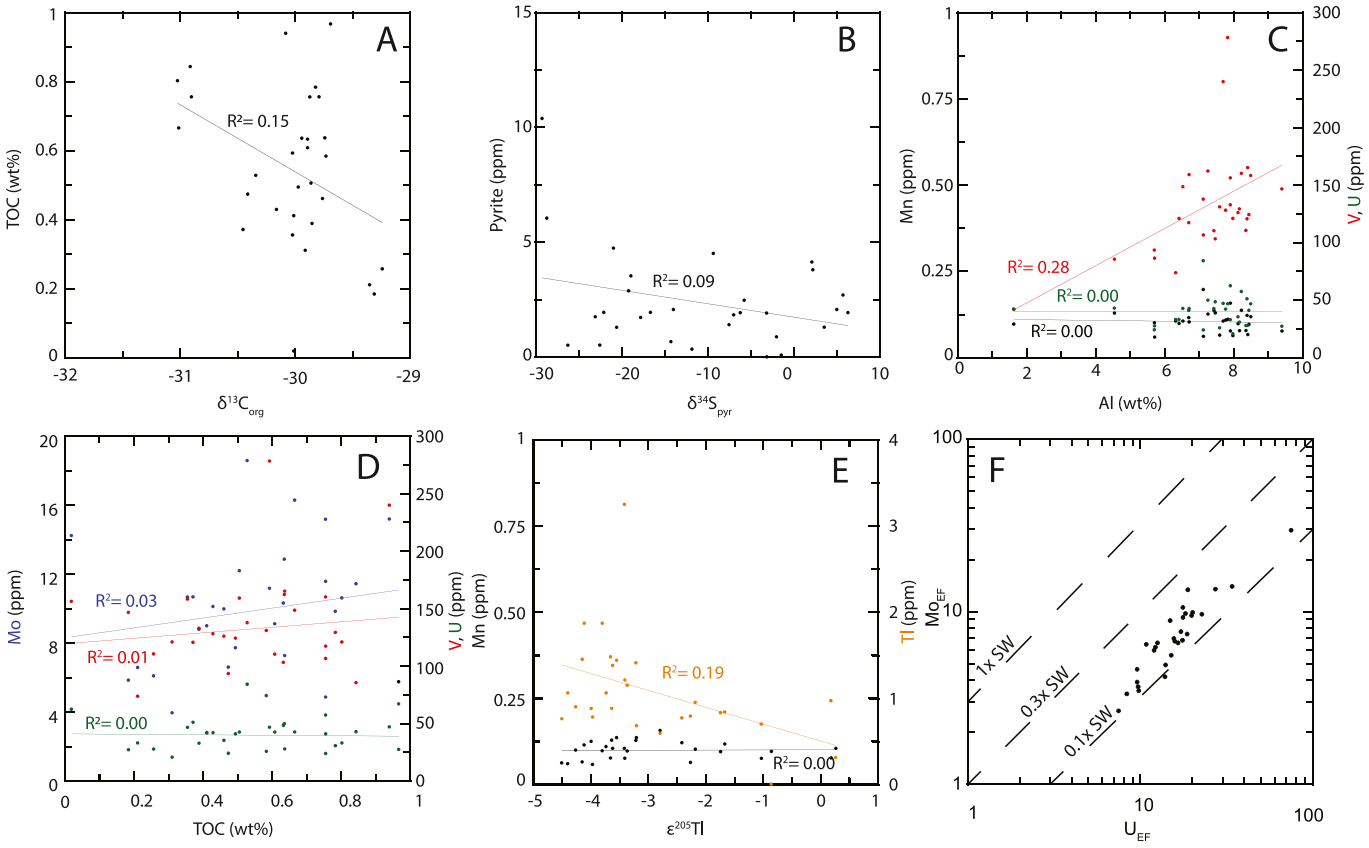

Fig. 3. Cross plots of geochemical data used to assess potential diagenetic alteration. All red circles and trend lines correspond the V concentrations, while yellow and blue circles/trend lines correspond to U and Mo concentrations respectively, in panels C and D. Orange circles and trendlines correspond to Tl concentrations in panel E. (For interpretation of the references to colour in this figure legend, the reader is referred to the web version of this article.)

positions within their respective continental margins and hydrographic settings. Thus, these similar trends in sulfur isotopes, (i.e., near synchronous change in the same negative direction) indicate that sedimentary pyrite records from Röstånga-2 were primarily the result of fluctuations in global pyrite burial rates, rather than local processes. While we cannot unambiguously eliminate diagenetic alteration and local influences, these processes seem limited, and thus we evaluate changes in paleoredox proxies as mostly reflecting primary seawater conditions. We will first discuss the iron speciation, $\delta^{34}S_{pyr}$, Mn and Mo concentrations within the context of local marine paleoredox conditions in the Baltoscandian paleobasin. With local paleoredox conditions constrained, we then interpret changes in V and U concentrations and Tl isotopic compositions to reflect changes in the global extent of anoxia. Finally, these combined local and global perspectives of marine oxygenation will be linked to well-established Ordovician biodiversification trends.

5.1. Local redox conditions within the Baltoscandian paleobasin

Throughout the Röstånga-2 drill core, iron geochemistry shows Fe_{HR}/Fe_T values mostly above the 0.22 threshold (Fig. 2), but not above the 0.38 threshold. This may indicate potential complications in determining the local redox conditions of this basin. Fe_{HR}/Fe_T values that fall between 0.22 and 0.38 are considered ambiguous, possibly anoxic, through experimentation using modern anoxic marine analogs (Raiswell et al., 2018). Modern and ancient studies with values within these ranges are either a result of high sedimentation rates, that may dilute the highly reactive fraction of iron, or sections that may have experienced extensive diagenesis that transformed highly reactive iron to the silicate fraction (Raiswell et al., 2018). Although our various geochemical cross-plots suggest that the extent of diagenetic overprinting is limited, the quantity of highly reactive Fe transferred into silicate Fe is under-constrained without further mineralogical data. Meanwhile, Fe_{pyr}/Fe_{HR} values plot consistently above the euxinic, 0.8, threshold apart from a handful of outliers, suggesting that nearly all Fe within the study area was pyritized. This, in turn, suggests that at minimum, sulfidic pore waters were present during the time of deposition. The Röstånga-2 drill core contains one of the most expansive Darriwilian–Sandbian black shale dominated sections in the study region, and thus siliciclastic dilution of highly reactive iron is likely. Indeed, we find that the Röstånga-2 drill core has a relatively high calculated linear sedimentation rate of ~8 m/Myr, which may create artificially lower Fe_{HR}/Fe_T values, falsely indicating deposition under oxic marine conditions due to siliciclastic dilution. Many Phanerozoic black shales have significantly lower calculated sedimentation rates (typically between 0.5 and 2.5 m/Myr) than those calculated for the Röstånga-2 drill core, which is consistent significant siliciclastic dilution being a major influence on our Fe speciation results (Ibach, 1982). The use of Fe_T/Al ratios is a common tool to correct for dilutions of Fe in siliciclastic rocks. Our observed Fe_T/Al values (Röstånga-2 average = 0.46) mostly fall within the average for Paleozoic marine shales, which is $Fe_T/Al = 0.53 \pm 0.11$ (Raiswell et al., 2018). The combined Fe geochemical data suggest that the Röstånga-2 drill core was deposited in a marine setting with reducing bottom waters and fairly high sedimentation rates (Raiswell et al., 2018).

Trace metal concentrations of Röstånga-2 drill core can further aid in the determination of local paleoredox conditions throughout the Middle–early Late Ordovician. Concentrations of Mn are used to identify potential reducing conditions, as Mn is highly redox-sensitive and enrichment (or lack thereof) can be a powerful indicator of marine redox conditions. Here we observe average Mn concentrations of <1 ppm, well below the average modern oxic shelf environments (~850 ppm), indicating that anoxic conditions were likely present throughout deposition of the core succession (Taylor and McLennan, 1981; Maynard and Force, 1991; Taylor and McLennan, 1995). Additionally, the concentrations of other redox-sensitive metals that respond to anoxic, but non-sulfidic conditions, such as V and U, show moderate enrichments (enrichment factors of ≥3) beyond the upper continental crust (UCC) values (Fig. 2) for these trace metals (UCC = 60 and 2.8 for V and U, respectively) suggesting that this analyzed section of the Baltoscandian paleobasin was likely anoxic during the time of deposition (Taylor and McLennan, 1981; Taylor and McLennan, 1995). Iron speciation, specifically Fe_{pyr}/Fe_{HR} ratios, in combination with concentrations of Mo (see more below), suggest sulfidic pore waters underlying anoxic marine bottom waters, as Fe_{pyr}/Fe_{HR} values that are persistently above 0.8 through most of the core and [Mo] that are mildly enriched (enrichment factors ≥3) above UCC values (Fig. 2).

Additionally, our new $\delta^{34}S_{pyr}$ values show correspondingly heavy values (~ + 0.5‰ average, with a maximum value of ~ + 6‰) in the upper *H. lentus* through *Pt. elegans* biozones of the Röstånga-2 drill core. This may indicate locally elevated MSR rates and resultant increased local pyrite burial rates, which is supported by the ubiquitous distribution of finely disseminated pyrite in the core. Throughout the Röstånga-2 drill core, we have identified mild enrichments of Mo (<25 ppm), which is not necessarily indicative of euxinic bottom-water conditions, but rather indicates sulfide buildup contained within sediment porewaters (Scott and Lyons, 2012; Hardisty et al., 2018). However, as discussed above, the high sedimentation rates that may have diluted the iron speciation values may also be responsible for diluting the authigenic enrichment of other redox-sensitive trace metals such as Mo, and to a lesser extent, V and U as these elements contain a higher UCC concentration (Tribovillard et al., 2006; Scott and Lyons, 2012).

While the location of sulfide production may be a factor in controlling Mo enrichments, the connectivity to open marine conditions may also have played a role in modulating Mo concentrations. The degree of basin restriction affects water mass renewal times, which in turn affects the marine reservoir size of a given analyzed trace element, which will result in a low authigenic enrichment (Algeo and Lyons, 2006; Scott et al., 2008; Scott and Lyons, 2012). Cross plots between the enrichment factors of Mo_{EF} and U_{EF} are suggested to be a tool to evaluate the degree of restriction and the evolution of paleoredox conditions (Algeo and Tribovillard, 2009). Deviation from the modern seawater molar ratio of Mo/U of ~7.5–7.9 towards lower ratios (~0.3–0.5) indicates authigenic enrichment under increasingly Mo depleted water masses, potentially due to the reservoir effect (Tribovillard et al., 2008; Algeo and Tribovillard, 2009). The overall lower values of Mo_{EF} and U_{EF} found in the Röstånga-2 drill core potentially reflect some degree of restriction to the basin (Fig. 3F), but complete restriction is unlikely. The preservation of open-marine, pelagic graptolite faunas throughout the entire core (Maletz et al., 2020) indicates at least a surficial exchange of open-marine waters. The connectivity to open marine conditions is indicated by synchronous shifts in $\delta^{18}O$ and $\delta^{13}C$ records from nearby sections from the same basin (Rasmussen et al., 2016; Edward et al., 2022), as well as the MDICE that has been previously identified in $\delta^{13}C_{org}$ records from this drill core (Bergström et al., 2020). Additionally, our $\varepsilon^{205}Tl$ data we present are not dominated by values that are representative of input values, a basin restriction scenario that has been documented in Tl isotopic trends in the modern Black Sea (Owens et al., 2017). While not completely constrained, the degree of restriction may just be limited to an intermediate–shallow sill that prevented full bottom water exchange with open-marine conditions.

5.2. Signatures of global marine paleoredox responses throughout the Middle–Late Ordovician

With local paleoredox conditions within the Baltoscandian paleobasin constrained by Fe speciation, enrichments of redox sensitive trace metals and depletion of Mn, we can now use our Tl and pyrite sulfur isotope datasets to interpret changes in the global burial flux of Mn-oxides and pyrite. Thus, these two biogeochemical trends have the potential to reflect global fluctuations in Ordovician marine redox conditions. Our Tl isotopic profile shows heavy values, at or beyond Tl input values to the modern oceans (Owens, 2019), in the *H. lentus* graptolite

Biozone and progressively trends towards isotopically lighter values throughout the uppermost Darriwilian (*Pt. elegans* Biozone and upward), which we interpret as a shift towards enhanced formation and burial of Mn-oxides resulting from progressive oxygenation of the global oceans. Globally pervasive reducing marine conditions in the early Darriwilian (*H. lentus* Biozone) were likely the primary cause of the heavy Tl isotopic values compared to the isotopically light modern ocean ε^{205}Tl values of −6 (Owens et al., 2017). It is important to note that the observed shift towards lighter Tl isotopic values can also be controlled by Tl burial into the alteration of oceanic crust (AOC) on timescales greater than ~5 Myr, where this output flux is thought to have an increased significance (Nielsen et al., 2009; Coggon et al., 2014; Owens et al., 2017). Our study interval encompasses ~11 Myr (middle of the *H. lentus* to the top of the *N. gracilis* biozone), with the detailed graptolite biostratigraphy from Maletz et al. (2020) and age calibrations of these specific biozones based upon the latest Geologic Time Scale from Goldman et al. (2020). Therefore, AOC may play a greater role in controlling Tl isotopic trends than studies focused on singular, short lived events (i.e., ≤ 1Myr) in Earth history (Ostrander et al., 2017; Them et al., 2018; Fan et al., 2020; Newby et al., 2021). AOC is generally associated with low temperature alteration of crustal material at mid ocean ridges; however, unambiguous proxies that can be used for determining the relative strength of this flux are underdeveloped. Increased mid-ocean ridge productivity can potentially drive changes in seawater stable Sr isotopes ($^{87}Sr/^{86}Sr$) to lower values, which is broadly consistent with the observed drop in $^{87}Sr/^{86}Sr$ isotopic values derived from well-preserved conodont elements throughout the Middle–Late Ordovician (Young et al., 2009; Saltzman et al., 2014; Edwards et al., 2015; Avila et al., 2022). Nevertheless, our observed negative Tl isotopic trend precedes the trend to lower $^{87}Sr/^{86}Sr$ isotopic values, thus suggesting that enhanced AOC may not be a primary driver of our Tl trend. Additionally, proxies utilized for silicate weathering (including $^{87}Sr/^{86}Sr$ and ε_{Nd}) have potentially identified enhanced weathering and resultant riverine input in chronstratigraphically correlative carbonates (Young et al., 2009; Conwell et al., 2022). This increase in riverine input is unlikely to influence the presented ε^{205}Tl record, as an increase towards bulk earth values of Tl ($\varepsilon^{205}Tl_{riv} = -2$) would produce a record towards more positive Tl values. However, this is the opposite of our observed data within the the Röstånga-2 drill core. Thus, we consider changes associated with weathering as a negligible influence on the ε^{205}Tl records. Inversely, we can compare active tectonic suture lengths as a first order estimate for changing mid-ocean ridge activity if we assume that total Earth volume did not significantly fluctuate during the geologically short analyzed (~11 Myr) interval. A relative increase in suture length should be inversely related to an increase in mid-ocean ridge activity to accommodate enhanced plate subduction. A noted increase in active suture lengths throughout the Middle Ordovician is thought to reflect the ongoing Taconic Orogeny along the eastern margin of Laurentia, and thus the influence of this flux may play a non-negligible role in controlling marine Tl isotopic compositions (Macdonald et al., 2019). These suture lengths and associated plate subduction rates are highly dependent on paleogeographic reconstructions and the preservation of obducted ophiolites, and at best can only be used as first-order estimations of mid-ocean ridge activity. Ultimately, identifying the total extent of AOC influence on our Tl isotopic trends remains elusive and may alter the total estimated extent of well-oxygenated seafloor area that is discussed below.

Recent mass balance calculations for another negative Tl isotope excursion surrounding the Neoproterozoic (Ediacaran) Shuram $\delta^{13}C$ excursion estimate that a Tl isotopic shift from $\varepsilon^{205}Tl = \sim 0$ to −5 would require a significant change in the strength of the AOC flux of ~25 to 30% (Ostrander et al., 2020). While a significant change in the AOC flux is possible over our ~11 Myr study interval, this is on the lower end of the duration of seafloor spreading rates that control second-order sea level cycles at ~1 to 100 Myr timescales (Miller et al., 2005; Haq and Schutter, 2008). Additionally, changes in the AOC flux would occur over a longer geologic time scale (multi-million years to tens of million years), while rapid fluctuations (less than ~5 million years) in Mn-oxide burial would be superimposed onto these long-term trends and thus cannot be the sole mechanism driving the observed Tl isotopic profile. The extent of control that AOC has on our Tl isotopic trends is currently under-constrained, however changes in marine oxygen contents have been proposed to have been a major factor for biodiversity changes in the Ordovician. Several models have attempted to reconstruct changes in atmospheric oxygen, and have predicted that an increase in pO_2 did occur in the Middle Ordovician, consistent with the trends in our Tl isotope dataset being interpreted as driven primarily by an increase in Mn-oxide burial in the Darriwilian (Edwards et al., 2017; Krause et al., 2018; Lenton et al., 2018). Furthermore, there are several global marine redox proxy datasets that span this time interval from carbonate settings indicating potential changes in the global marine redox conditions during the Middle Ordovician (see below for more detailed discussion; Young et al., 2016; del Rey et al., 2022).

The changes in global Mn-oxide burial rates inferred from our Tl isotopic trends can subsequently be used to infer first-order trends in the global extent of anoxia in the Middle–Late Ordovician. Previous studies have estimated that ~95% of the modern sea floor area are considered oxygenated to allow burial of authigenic Mn-oxides, and conversely ~5% of modern sea floors are considered anoxic (Meile and Van Cappellen, 2003; Thullner et al., 2009; Reinhard et al., 2013). As a result of widespread Mn-oxide burial within well-oxygenated settings, and a minor contribution of AOC, modern seawater Tl isotopic compositions are at −6 (Owens et al., 2017; Ostrander et al., 2020). In deep sea settings, oxygenated seafloor extent is estimated to bury between 0.7 and 2.6 Gt of Mn in the forms of crusts and nodules (Broadus, 1987; Meile and Van Cappellen, 2003; Thullner et al., 2009). A recent study has, however, identified that non-crystalline microparticles of Mn-oxides may be an additional factor to the global Mn budget (Uramoto et al., 2019). Regardless of the absolute flux of Mn-oxide burial in modern marine settings, based on our reasoning above, we interpret that our Middle–Late Ordovician geochemical trends primarily reflect changes in the global Mn-oxide burial. A recently published Tl isotope mass balance model has identifed three major mechanisms that exert primarily controls on marine Tl isotopic compositions, Mn-oxides that are deposited beneath well-oxygenated bottom waters (f_{oxic}), low temperature hydrothermal alteration associated with AOC (f_{AOC}), and sediments that are deposited beneath anoxic bottom waters (f_{anoxic}) (Ostrander et al., 2020). This mass balance explores all possible flux strength combinations to reproduce possible Tl isotopic excursions found in the geologic record. Utilizing this mass balance model of Tl isotopes, to produce a contemporaneous sea-water Tl isotopic value = −2 found in the Röstånga 2 drill core, virtually no Mn-oxide burial can occur in marine sediments, e.g., f_{anoxic} is the dominant mechanism exerting control on seawater Tl isotopic compositions, while f_{AOC} plays a minor role (Ostrander et al., 2020). Using the same mass balance model discussed above, and assuming that Mn-oxide burial flux scales directly with oxygenated seafloor area, along with a similar starting Mn marine reservoir, we estimate that Middle–Late Ordovician Mn-oxide burial fluxes (e.g., f_{oxic}) increased by ~15–25% at the expense of f_{anoxic} to produce the minimum Tl isotopic values of ~ − 5. In this estimation, we also assume that no major contemporaneous changes in f_{AOC} occurred; however a decrease in f_{AOC} at the expense of f_{anoxic} would ultimately decrease the estimated extent of reducing conditions. If we assume that changes in Mn-oxide are correlated with the extent of oxic seafloor, we estimate ~10–15% of early Darriwilian marine settings (where $\varepsilon^{205}Tl = -2$) were sufficiently oxygenated to bury Mn-oxides, and transiently progressed to ~80% of seafloor area being sufficiently oxygenated to bury Mn-oxides by the late Darriwilian–early Sandbian (where $\varepsilon^{205}Tl = -5$). These estimates likely represent an oversimplification in the causal factors responsible for changes in Tl isotopic compositions, such as the absolute strength of Mn-oxide burial and changes in oxic sea floor extent. However, these estimates represent a first-order quantification of

seafloor oxygenation during the Middle Ordovician – and according to these results, substantial changes in the extent of seafloor oxygenation coincide with peak faunal richness in all major marine taxa.

Our new $\delta^{34}S_{pyr}$ profile from the Röstånga-2 drill core shows similar first-order trends to $\delta^{34}S_{CAS}$ found in Laurentian, South Chinese and Argentine Precordilleran margins. These changes in $\delta^{34}S_{CAS}$ values generally show a ~ 12‰ to ~15‰ negative excursion leading into the MDICE interval (Fig. 4), with a return to baseline or heavier values in the lower Sandbian (Thompson and Kah, 2012; Kah et al., 2016; Young et al., 2016; Edwards et al., 2019; Kozik et al., 2019). While the Röstånga-2 drill core utilizes graptolite biostratigraphy and Laurentian margins utilize conodont biostratigraphy, we can correlate these successions with reasonable confidence using the latest global biostratigraphic schemes that integrate fine-grained clastic with carbonate facies biozonations (i.e., Goldman et al., 2020). These sulfur isotopic datasets show remarkably similar and synchronous changes in terms of magnitude and direction, suggesting that first-order changes in global sulfur cycling affected Baltic margins as well. Pyrite sulfur isotopic compositions are influenced by a variety of factors, ranging from sedimentation rate, oxygen penetration depths, seawater sulfate concentration, type and abundance of organic matter and reactive iron, and MSR rate (Lang et al., 2020; Pasquier et al., 2021). A sufficiently large marine sulfate reservoir is required for pyrite sulfur isotopic compositions to mirror contemporaneous seawater sulfur isotope values, which can be recorded by $\delta^{34}S_{CAS}$ (Gomes and Hurtgen, 2015; Kah et al., 2016; Canfield, 2019). Several estimations for seawater sulfate concentrations have been made utilizing a variety of methods, and ultimately produce a range from 2 to 15 mM throughout the Ordovician (Horita et al., 2002; Algeo et al., 2015; Kah et al., 2016; Young et al., 2016). The negative shift in $\delta^{34}S_{CAS}$ datasets seen in Middle Ordovician sections has largely been attributed to a global reduction in reducing marine conditions, and thus a reduction in pyrite burial, which ultimately increased coeval seawater sulfate concentrations (Thompson and Kah, 2012; Kah et al., 2016; Young et al., 2016). Due to the similarity in timing, magnitude and directionality of sulfur isotopic change in $\delta^{34}S_{CAS}$ from western and eastern Laurentia, Argentine Precordillera, and South China with our new $\delta^{34}S_{pyr}$ dataset from Baltica, we interpret these records to reflect changes in global marine paleoredox conditions (Kah et al., 2016; Young et al., 2016). With this framework in mind, we can now interpret changes in Tl isotopic compositions, as well as $\delta^{34}S_{CAS}$, as global indicators for paleoredox changes associated with the peak faunal diversity interval of the GOBE.

An increase in marine oxygenation associated with changes in global ocean circulation patterns has been previously proposed to explain several of the biodiversity and geochemical trends in the Middle–Upper Ordovician, including changes in $\delta^{34}S_{CAS}$ (Kah et al., 2016; Rasmussen et al., 2016; Young et al., 2016; Kozik et al., 2019). This ventilation and subsequent marine oxygenation is likely responsible for the large negative excursion (~12‰) in $\delta^{34}S_{CAS}$ (discussed above) in Darriwilian carbonate platform settings associated with the MDICE interval (Thompson and Kah, 2012; Kah et al., 2016; Young et al., 2016). This excursion in $\delta^{34}S_{CAS}$ has been interpreted as a global reduction in pyrite burial during the Middle Ordovician, possibly due to ventilation and cooling of sea surface temperatures (SSTs). Young et al. (2016) constructed a simple forward box model to quantify changes in ancient fluxes (including altering riverine input, pyrite burial rates and the fractionation factor between reactant sulfate and product sulfide, i.e., $\Delta^{34}S$) needed to reproduce the observed $\delta^{34}S_{CAS}$ trends and ultimately, concluded that a reduction in the pyrite burial flux between 18 and 45% was responsible for the secular change in seawater sulfate isotopic compositions. Here we build upon these previously published datasets in an attempt to add a first-order quantification on the shrinking areal extent of global seafloor with highly reducing conditions (e.g., euxinia) throughout the Middle–Late Ordovician. Additionally, this study estimates that the pre-excursion pyrite burial flux was significantly higher (Middle Ordovician $F_{pyr} = 1.1 \times 10^{18}$ mol S/Myr) than a modern flux of 0.67×10^{18} mol S/Myr (Young et al., 2016). In modern marine settings, euxinia is estimated to occupy ~0.15% of the total seafloor area, and the corresponding global reduced sulfur burial rate is estimated to be ~3.1 $\times 10^{16}$ mol S/Myr, most of which is buried within the euxinic Black Sea (Neretin et al., 2001; Reinhard et al., 2013). This burial of reduced S includes pyrite burial as well as intermediate species and organically bound S, and thus our calculations likely overestimate changes in the euxinic conditions. Importantly, our calculation of the extent of euxinic conditions presented here does not account for changes in $\Delta^{34}S$, which can aid in modulating the changes in pyrite burial fluxes needed to reconstruct changes in $\delta^{34}S_{CAS}$. In these calculations we assume that this reduction in pyrite burial flux occurs primarily in euxinic settings, and not in reducing, but non-euxinic settings. We estimate that the extent of euxinic conditions in the early Darriwilian was ~35% more than the modern extent, equating to approximately 5.3% of the Ordovician marine bottom waters experiencing euxinia. The subsequent ~18–45% reduction in global pyrite burial as estimated by Young et al. (2016) in the mid-Darriwilian would then reduce the maximum global estimate of euxinia to ~4.3–0.1% in the late Darriwilian. We reiterate that these estimates represent solely changes in pyrite burial, and that changes in the riverine flux and/or changes in the fractionation factor between sulfate and product sulfide could alter these estimates, as shown in a recent study on the Upper Ordovician (Kozik et al., 2022).

Other paleoredox proxy studies have provided additional support for the dynamic change in marine oxygen levels we interpret to have occurred during the Middle Ordovician. A recent study compiling iron geochemistry from several hydrographically dispersed paleocontinents has identified that a significant proportion of iron speciation datasets from the Lower–Middle Ordovician (Floian to early Darriwilian stages) were largely deposited under anoxic conditions, but many of the datasets identify less reducing conditions during the Late Ordovician (Sandbian Age), as part of a prolonged trend towards more modern, well oxygenated Earth systems (Sperling et al., 2021). A recent study utilizing uranium isotopes ($\delta^{238}U_{carb}$) from a carbonate-dominated Baltic sequence has claimed that marine oxygenation was likely not a major driver of the GOBE (del Rey et al., 2022). This study interprets the relatively invariant $\delta^{238}U_{carb}$ within the latest Dapingian through the earliest Darriwilian (Dp3–Dw1 stage slices) as stable paleoredox conditions, that coincided with peak diversification rates associated with the GOBE. This study subsequently identified a long term trend towards heavier $\delta^{238}U_{carb}$ values within the latest Darriwilian (Dw3 stage slice), following the onset of the highest rates of diversification found in Baltica and Laurentia (Kröger et al., 2019; Rasmussen et al., 2019; del Rey et al., 2022). This overall trend towards more oxygenated marine environments throughout the Darriwilian to earliest Sandbian is ultimately consistent with our Tl isotopic trends and interpretations. Other nontraditional geochemical records that utilize $\delta^{98}Mo$ have identified shifts to heavier values in the Middle Ordovician, and interpreted this to reflect a shift towards more oxygenated deep marine settings (Dahl et al., 2010; Lenton et al., 2016). Collectively, these multiple lines of independent geochemical evidence, in conjunction with our newly identified long-term negative Tl isotopic shift confirm that an increase in global marine oxygenation coincided with cooler global SSTs and climate during this interval of the Middle Ordovician (Trotter et al., 2008; Goldberg et al., 2021; Edwards et al., 2022). Based on the collective evidence discussed here, the peak rate in diversification occurs within the Dapingian–earliest Darriwilian, while the long term oxygenation trends are likely linked to the interval of peak faunal richness in the Middle–Late Ordovician (Fig. 4).

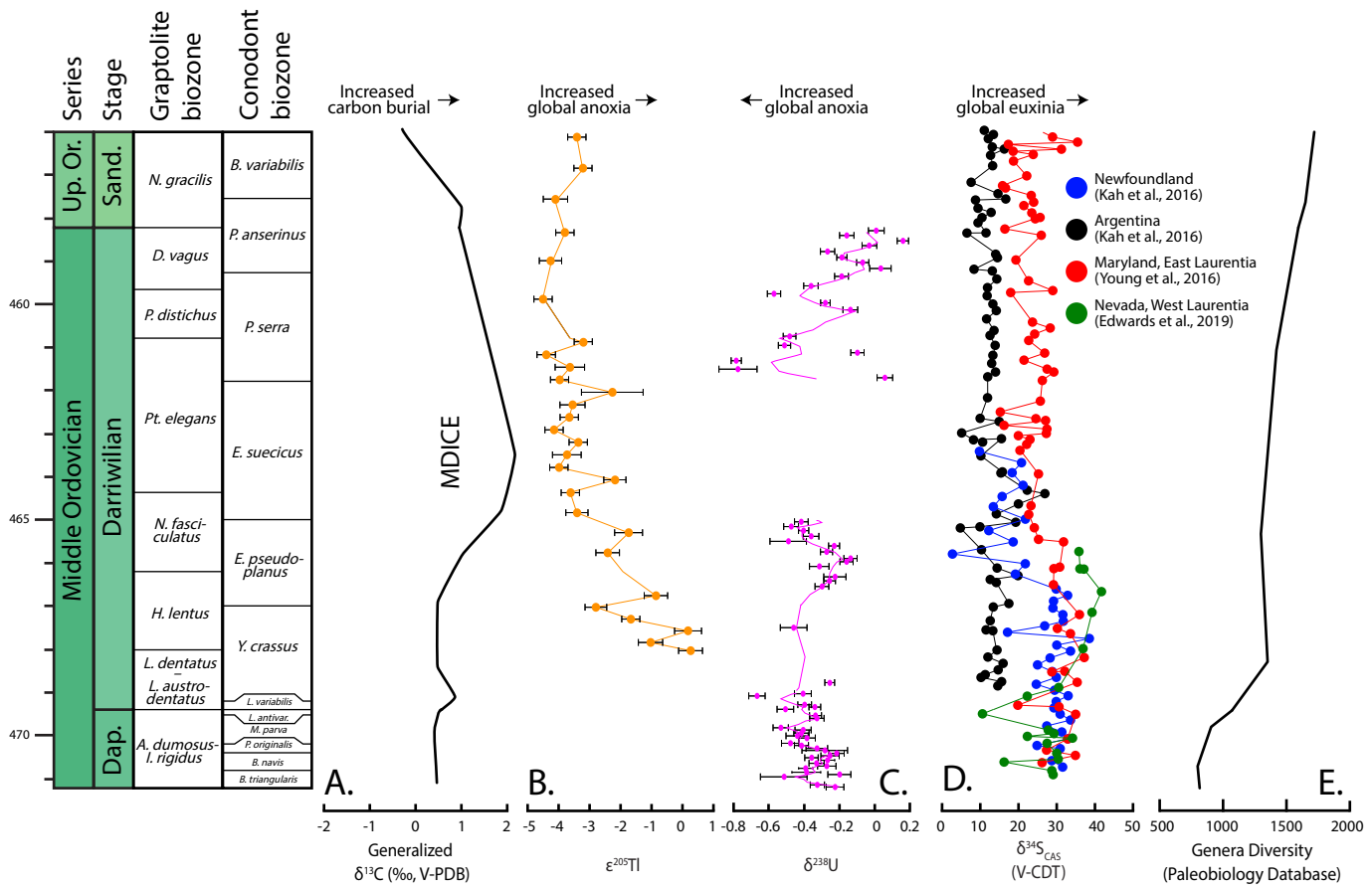

Fig. 4. Generalized global seawater geochemical trends throughout the Middle–Late Ordovician. A, Generalized Middle–Late Ordovician $\delta^{13}C_{carb}$ profile (adapted from Cramer and Jarvis, 2020). B, $\varepsilon^{205}Tl$ data (this study) that can be used to interpret changes in global marine anoxia (Mn-reduction). C, Replotted data and trends in $\delta^{238}U_{carb}$ used to interpret changes in global marine anoxia (Fe-reduction), replotted from del Rey et al. (2022). D, Replotted data and trends in $\delta^{34}S_{CAS}$ used to interpret changes in global euxinia (SO_4-reduction), replotted from Young et al. (2016), Kah et al. (2016), and Edwards et al. (2019). E, Changes in generic diversity modified from Rasmussen et al. (2019).

5.3. Paleoredox changes coincide with peak rates of Ordovician biodiversification

Our new Tl isotopic trends reveal a steady increase in bottom water oxygen levels which may have fueled the peak rates of marine biodiversification in the Middle Ordovician. This expansion in oxic conditions likely contributed to the increased ecosystem complexity and biodiversity as more shelf areas and epicontinental seaways became increasingly oxygenated (Rasmussen et al., 2019; Stigall et al., 2019). Using the Paleobiology Database, Rasmussen et al. (2019) found a strong correlation between increases in modeled atmospheric pO_2 levels, lowering global average temperature and generic richness, however the increase in biodiversity found in this study preceded the increase in oxygenation. Our new global marine redox proxy dataset provides independent lines of evidence that significant changes in marine oxygen levels (based on changes in $\varepsilon^{205}Tl$) and global euxinia (based on changes in $\delta^{34}S_{CAS}$) align closely with changes in marine biodiversity records generated from the Paleobiology Database (Fig. 5). Interestingly, our geochemical proxy data do not reflect biodiversification patterns from datasets compiled from other paleocontinents, such as South China (Deng et al., 2021). If indeed changes in marine oxygenation were a primary controlling factor in the timing and rate of peak Ordovician diversification, spatial heterogeneities in paleoredox conditions due to differences in upwelling and paleocurrents linked to dynamic global cooling, may ultimately be an important contributing factor for these discrepancies. This may be exceedingly prevalent in high latitude settings, i.e., Gondwanan and peri-Gondwanan margins in the southern hemisphere, as this cooling trend may have enhanced dissolved oxygen content at sites of deep water formation (Rasmussen et al., 2016).

The changes in oxygenation were plausibly linked with cooling global climate conditions during the Middle Ordovician, a time interval in which surface and deep water currents may have been altered due to cooling SST's (Trotter et al., 2008; Rasmussen et al., 2016; Pohl et al., 2017; Edward et al., 2022; Edwards et al., 2022). The establishment of cooler SSTs (within the modern equatorial range) during the Middle Ordovician possibly signals the start of icehouse conditions that eventually led to Gondwanan glaciation in the Late Ordovician (Trotter et al., 2008; Edwards et al., 2022). This overall cooling trend may be reflected in the rapid, third-order sea level fluctuations observed throughout the Middle Ordovician (Haq and Schutter, 2008). The shift towards isotopically light $\varepsilon^{205}Tl$ values in the early Darriwilian is coincident with minima in global sea level records for the Middle Ordovician, suggesting a very plausible connection between marine oxygenation and global climate. These connections between marine oxygen, global climate and sea level reflect synergistic effects, wherein global cooling enabled more dissolved oxygen incorporation within marine waters. We envision that thermohaline circulation intensified as a result of enhanced deep-water formation around polar Gondwanan margins (e.g., Pohl et al., 2022), leading to increased renewal of deep-water oxygenation throughout our studied time interval, as seen with our Tl isotopic trends. Importantly, our Tl isotope data are consistent with recent global modeling of upper oceanic oxygen for this interval of the Ordovician (Pohl et al., 2022). Ultimately, Middle Ordovician cooling would have allowed for enhanced oxygen solubility during deep-water formation, and the

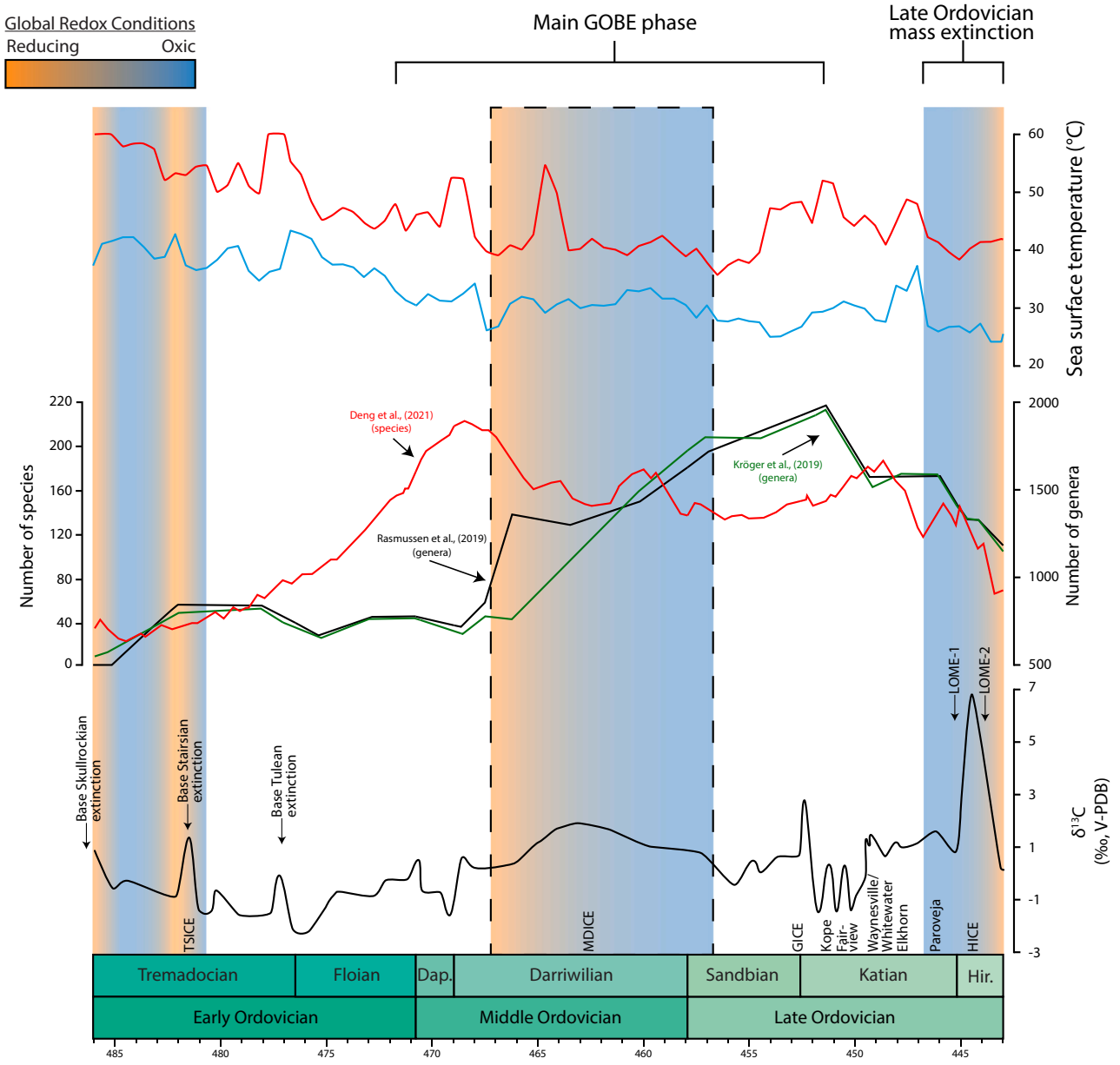

Fig. 5. Generalized biodiversity trends throughout the Ordovician and its relationship to known changes in carbon cycling, paleoredox and temperature. Generalized $\delta^{13}C_{carb}$ profile is adapted from Cramer and Jarvis, (2020), with noticeable carbon isotopic excursions superimposed below and noticeable extinctions above the $\delta^{13}C_{carb}$ profile. Faunal diversity curves from separate paleontological databases are compared to fluctuating paleoredox conditions and temperature (diversity curves adapted from Kröger et al., 2019; Rasmussen et al., 2019; Deng et al., 2021). Axis on the left (Number of Species) is used for changes in diversity presented by Deng et al. (2021), while the axis right (Number of Genera) is used for changes in diversity presented by Rasmussen et al. (2019) and Kröger et al. (2019). Generalized changes in temperature is adapted from Goldman et al. (2020) and Trotter et al. (2008). Predominant global paleoredox state of Ordovician marine settings are indicated by shading of several intervals, with orange shading representing predominantly reducing conditions, and blue shading representing more oxic conditions (Hammarlund et al., 2012; Thompson and Kah, 2012; Young et al., 2016; Bartlett et al., 2018; Edwards et al., 2018, 2019; Edwards, 2019; Kozik et al., 2019, 2022, 2023; Dahl et al., 2021). This study's interval is represented by the dashed box outlining the Middle–earliest Late Ordovician. (For interpretation of the references to colour in this figure legend, the reader is referred to the web version of this article.)

invigorated thermohaline circulation led to increased marine ventilation as indicated by our negative Tl isotopic trend, likely corresponding to an increase in Mn-oxide burial under expanding oxic conditions globally.

Previous studies have identified that faunas with different life modes (i.e., planktonic, nektonic, benthic) diversified asynchronously in the Ordovician, with planktonic faunas diversifying before and at a faster rate than those with a benthic mode of life (Servais et al., 2010; Stigall et al., 2019; Deng et al., 2021). These diversification patterns may be intimately related to the evolving paleoredox landscape, as a protracted and/or episodic ventilation of Ordovician oceans may have affected marine shelves and continental margins differently in hydrographically separated regions. Recent comparisons of Ordovician biodiversity datasets also indicate that marine animal diversification was heterogeneous with respect to different paleocontinents i.e., Laurentian/Baltic and South China diversity trajectories (Stigall et al., 2019; Servais et al., 2021; Deng et al., 2021). While our new Tl isotopic records, or the sulfur isotope records discussed above, cannot specifically identify where the oxygenation was occurring in Ordovician oceans, these proxies do

indicate that there was an enhanced capacity to bury more Mn-oxides. This suggests that large swaths of marine sea floors transitioned from highly reducing conditions to less reducing (and inversely, the capacity to form and bury pyrite was diminished based on sulfur isotope records). Currently, we are unaware of any published temporally equivalent proxy dataset to the one present here, that can confidently support global changes in upper water column redox conditions (e.g., iodine-to-calcium ratios, or unambiguous trace metal concentration trends). Regardless, the diversification of planktonic groups such as chitinozoans, acritarchs, and graptolites during the Floian–Dapingian, suggests that water-column oxygen contents may have increased due to a reorganization in thermohaline currents (Rasmussen et al., 2016; Pohl et al., 2017; Stigall et al., 2019), prior to bottom-water oxygenation in the middle–late Darriwilian that coincided with diversification of benthic groups (e.g., brachiopods, corals, echinoderms, bryozoans). Following this potential oxygenation of Ordovician water columns, our new Tl isotopic record alongside trends in sulfur isotopic compositions (i.e., $\delta^{34}S_{CAS}$ and $\delta^{34}S_{pyr}$), suggest that bottom water conditions, and thus oxygen penetration into sediments may have increased, allowing epi- and infauna to diversify later in the Darriwilian–Sandbian. With this mounting evidence that paleoredox was indeed changing throughout the Middle–Late Ordovician through enhanced burial of Mn-oxides, (and a reduction of pyrite burial), these changes are likely intimately related to ecospace restructuring and the increase in biodiversity found in this interval. This increase in oxygen availability allowed for enhanced predation as high trophic level fauna have a higher oxygen quota, as is evident from the increase in bioerosion structures in Middle–Late Ordovician strata (Fig. 4F) (Buatois et al., 2016). Secondly, this expansion of oxygenated conditions likely produced deeper oxygen penetration into sediments due to the suppression of sediment chemoclines, allowing for benthic organisms such as gastropods and bivalved fauna to increase burrowing depths which would contain previously inaccessible, labile organic matter, especially evident in deep-marine bioturbation structures (Buatois et al., 2016; Buatois and Mángano, 2018). This new food source either in sediments or through predation, may then have fostered new ecospaces fueling the biodiversification patterns throughout the GOBE.

6. Conclusions

Our new multiproxy dataset includes pyrite sulfur isotopes, iron speciation, trace element concentrations and Tl isotopic records from the Middle–Upper Ordovician in the Röstånga-2 drill core of Skåne (Scania), southern Sweden. It documents both local and global paleoredox conditions from an expansive Ordovician black shale succession of Baltica. Local bottom water paleoredox conditions are interpreted to have been predominantly anoxic throughout deposition of the Röstånga-2 core succession, and with sulfidic sediment porewaters likely throughout much of the study interval as indicated by the combination of iron speciation and molybdenum concentrations. Our new Tl isotopic dataset suggests a protracted increase in marine oxygenation through the Middle to Late Ordovician. This novel Tl isotopic record presents new evidence for expanding oxic marine conditions surrounding peak generic richness of marine animals in the Middle–Late Ordovician. Additionally, our new pyrite sulfur isotope records show nearly synchronous changes with Laurentian sulfur isotopic records (both CAS and pyrite), which suggest that global sulfur cycle changes are also recorded and reflected within the new records presented here. Our Tl isotope dataset supports the previous implications put forward for the coeval $\delta^{34}S_{CAS}$ studies from Laurentia, indicating that there was an overall reduction in globally reducing conditions throughout the Darriwilian–Sandbian ages of the Middle–Late Ordovician. This transition to more oxic conditions in the Middle Ordovician oceans arguably was an important factor for the increased biodiversification in the peak interval of the GOBE. We attribute these shifts in paleoredox conditions to a cooling global average climate and a strengthening of thermohaline circulation which led to enhanced marine ventilation during the Middle Ordovician. With these newly ventilated areas and increased oxygen availability, sulfidic conditions were likely suppressed to greater depths below the sediment-water interface, thus facilitating further diversification of aerobic metabolic pathways, continued diversification and ultimately ecosystem reorganizations.

Declaration of Competing Interest

The authors declare that they have no known competing financial interests, nor personal relationships that could have influenced the work reported in this manuscript.

Data availability

Data will be made available on request. Supplementary data to this article can be found online at (https://doi.org/10.1016/j.gloplacha.2023.104183).

Acknowledgements

We would like to thank Sean Newby and Lindsi Allman for their assistance with geochemical analysis, and Frans Lundberg for assistance in sampling the Röstånga-2 drill core. We would also like to thank Linda Kah, Christian Rasmussen and an anonymous reviewer for their thoughtful and constructive comments that have considerably strengthened this manuscript, as well as Maoyan Zhu for his editorial guidance. The analytical work was performed at the National High Magnetic Field Laboratory in Tallahassee, Florida, which is supported by National Science Foundation Cooperative Agreement No. DMR-1644779 and by the State of Florida. This work was supported by the National Science Foundation Cooperative Agreement No. DMR-1157490 and the State of Florida. This research was funded by the Gyllenstierna Krapperup's Foundation (grant award KR2019-0089 to P. A. and S.A.Y.), the Birgit and Hellmuth Hertz Foundation (to A. L.), the NASA Exobiology Program (80NSSC23K0346 to S.A.Y. and J.D.O.), the Sloan Research Foundation (FG-2020–13552 to J.D.O), and the Winchester Fund (to N.P.K.).

Appendix A. Supplementary data

Supplementary data to this article can be found online at https://doi.org/10.1016/j.gloplacha.2023.104183.

References

Algeo, T.J., Lyons, T.W., 2006. Mo-total organic carbon covariation in modern anoxic marine environments: Implications for analysis of paleoredox and paleohydrographic conditions. Paleoceanography 21, 1–23. https://doi.org/10.1029/2004PA001112.

Algeo, T.J., Maynard, J.B., 2008. Trace-metal covariation as a guide to water-mass conditions in ancient anoxic marine environments. Geosphere 4, 872–887. https://doi.org/10.1130/GES00174.1.

Algeo, T.J., Tribovillard, N., 2009. Environmental analysis of paleoceanographic systems based on molybdenum-uranium covariation. Chem. Geol. 268, 211–225. https://doi.org/10.1016/j.chemgeo.2009.09.001.

Algeo, T.J., Luo, G.M., Song, H.Y., Lyons, T.W., Canfield, D.E., 2015. Reconstruction of secular variation in seawater sulfate concentrations. Biogeosciences 12, 2131–2151. https://doi.org/10.5194/bg-12-2131-2015.

Anbar, A.D., et al., 2007. A whiff of oxygen before the great oxidation event? Science 317, 1903–1906. https://doi.org/10.1126/science.1140325.

Avila, T.D., Saltzman, M.R., Adiatma, Y.D., Joachimski, M.M., Griffith, E.M., Olesik, J. W., 2022. Role of seafloor production versus continental basalt weathering in Middle to late Ordovician seawater $^{87}Sr/^{86}Sr$ and climate. Earth Planet. Sci. Lett. 593 https://doi.org/10.1016/j.epsl.2022.117641, 117641.

Bartlett, R., Elrick, M., Wheeley, J.R., Polyak, V., Desrochers, A., Asmerom, Y., 2018. Abrupt global-ocean anoxia during the late Ordovician–early Silurian detected using uranium isotopes of marine carbonates. Proc. Natl. Acad. Sci. U. S. A. 115, 5896–5901. https://doi.org/10.1073/pnas.1802438115.

Bergström, S.M., Huff, W.D., Koren, T., Larsson, K., Ahlberg, P., Kolata, D.R., 1999. The 1997 core drilling through Ordovician and Silurian strata at Röstånga, S. Sweden:

Preliminary stratigraphic assessment and regional comparison. Gff 121, 127–135. https://doi.org/10.1080/11035899901212127.
Bergström, S.M., Larsson, K., Pålsson, C., Ahlberg, P., 2002. The Almelund Shale, a replacement name for the Upper Didymograptus Shale and the Lower Dicellograptus Shale in the lithostratigraphical classification of the Ordovician succession in Scania, southern Sweden. Bull. Geol. Soc. Den. 49, 41–47. https://doi.org/10.37570/bgsd-2003-49-04.
Bergström, S.M., Chen, X., Gutiérrez-marco, J.C., Dronov, A., 2009. The new chronostratigraphic classification of the Ordovician System and its relations to major regional series and stages and to $\delta^{13}C$ chemostratigraphy. Lethaia 42, 97–107. https://doi.org/10.1111/j.1502-3931.2008.00136.x.
Bergström, S.M., Eriksson, M.E., Young, S.A., Ahlberg, P., Schmitz, B., 2014. Hirnantian (latest Ordovician) $\delta^{13}C$ chemostratigraphy in southern Sweden and globally: a refined integration with the graptolite and conodont zone successions. Gff 136, 355–386. https://doi.org/10.1080/11035897.2013.851734.
Bergström, S.M., Ahlberg, P., Maletz, J., Lundberg, F., Joachimski, M.M., 2018. Darriwilian (Middle Ordovician) chemostratigraphy linked to graptolite, conodont and trilobite biostratigraphy in the Fågelsång-3 drill core, Scania, Sweden. Gff 140, 229–240. https://doi.org/10.1080/11035897.2018.1466833.
Bergström, S.M., Ahlberg, P., Maletz, J., Lundberg, F., Joachimski, M.M., 2020. Integration of darriwilian (Middle ordovician) $\delta^{13}C_{org}$ chemostratigraphy with graptolite biostratigraphy in the classical Röstånga area in northwestern Scania (southern Sweden). Estonian J. Earth Sci. 69, 121–133. https://doi.org/10.3176/earth.2020.08.
Bowman, C.N., Young, S.A., Kaljo, D., Eriksson, M.E., Them, T.R., Hints, O., Martma, T., Owens, J.D., 2019. Linking the progressive expansion of reducing conditions to a stepwise mass extinction event in the late Silurian oceans. Geology 47, 968–972. https://doi.org/10.1130/G46571.1.
Broadus, J.M., 1987. Seabed Materials. Science 235, 853–860. https://doi.org/10.1126/science.235.4791.853.
Brüchert, V., Pratt, L.M., 1996. Contemporaneous early diagenetic formation of organic and inorganic sulfur in estuarine sediments from St. Andrew Bay, Florida, USA. Geochim. Cosmochim. Acta 60, 2325–2332. https://doi.org/10.1016/0016-7037(96)00087-7.
Buatois, L.A., Mángano, M.G., 2018. The other biodiversity record: Innovations in animal-substrate interactions through geologic time. GSA Today 28, 4–10. https://doi.org/10.1130/gsatg371a.1.
Buatois, L.A., Mángano, M.G., Olea, R.A., Wilson, M.A., 2016. Decoupled evolution of soft and hard substrate communities during the Cambrian explosion and Great Ordovician Biodiversification Event. Proc. Natl. Acad. Sci. U. S. A. 113, 6945–6948. https://doi.org/10.1073/pnas.1523087113.
Calvert, S.E., Pedersen, T.F., 1996. Sedimentary geochemistry of manganese; implications for the environment of formation of manganiferous black shales. Econ. Geol. 91, 36–47. https://doi.org/10.2113/gsecongeo.91.1.36.
Canfield, D.E., 2019. Biogeochemistry of sulfur isotopes. Stable Isot. Geochem. 43, 607–636. https://doi.org/10.1515/9781501508745-015.
Canfield, D.E., Raiswell, R., Bottrell, S.H., 1992. The reactivity of sedimentary iron minerals toward sulfide. Am. J. Sci. 292, 659–683. https://doi.org/10.2475/ajs.292.9.659.
Coggon, R.M., Rehkämper, M., Atteck, C., Teagle, D.A.H., Alt, J.C., Cooper, M.J., 2014. Controls on thallium uptake during hydrothermal alteration of the upper ocean crust. Geochim. Cosmochim. Acta 144, 25–42. https://doi.org/10.1016/j.gca.2014.09.001.
Conwell, C.T., Saltzman, M.R., Edwards, C.T., Griffith, E.M., Adiatma, Y.D., 2022. Nd isotopic evidence for enhanced mafic weathering leading to Ordovician cooling. Geology 50, 886–890. https://doi.org/10.1130/g49860.1.
Cramer, B.D., Jarvis, I., 2020. Carbon isotope stratigraphy. In: Geologic Time Scale 2020. Elsevier, pp. 309–343. https://doi.org/10.1016/B978-0-12-824360-2.00011-5.
Dahl, T.W., Hammarlund, E.U., Anbar, A.D., Bond, D.P.G., Gill, B.C., Gordon, G.W., Knoll, A.H., Nielsen, A.T., Schovsbo, N.H., Canfield, D.E., 2010. Devonian rise in atmospheric oxygen correlated to the radiations of terrestrial plants and large predatory fish. Proc. Natl. Acad. Sci. U. S. A. 107, 17911–17915. https://doi.org/10.1073/pnas.1011287107.
Dahl, T.W., Hammarlund, E.U., Rasmussen, C.M.Ø., Bond, D.P.G., Canfield, D.E., 2021. Sulfidic anoxia in the oceans during the Late Ordovician mass extinctions – insights from molybdenum and uranium isotopic global redox proxies. Earth Sci. Rev. 220 https://doi.org/10.1016/j.earscirev.2021.103748.
del Rey, Á., Rasmussen, C.M.Ø., Calner, M., Wu, R., Asael, D., Dahl, T.W., 2022. Stable Ocean redox during the main phase of the Great Ordovician Biodiversification Event. Commun. Earth Environ. 3, 220. https://doi.org/10.1038/s43247-022-00548-w.
Deng, Y., Fan, J., Zhang, S., Chen, Z., Shi, Y., Wang, H., Wang, X., Yang, J., Hou, X., Wang, Y., Zhang, Y., Chen, Q., Yang, A., Fan, R., Dong, S., Xu, H., Shen, S., 2021. Timing and patterns of the Great Ordovician Biodiversification Event and late Ordovician mass extinction: Perspectives from South China. Earth Sci. Rev. 220, 103743 https://doi.org/10.1016/j.earscirev.2021.103743.
Edward, O., Korte, C., Ullmann, C.V., Colmenar, J., Thibault, N., Bagnoli, G., Stouge, S., Rasmussen, C.M.Ø., 2022. A Baltic Perspective on the early to early late Ordovician $\delta^{13}C$ and $\delta^{18}O$ Records and its Paleoenvironmental significance. Paleoceanogr. Paleoclimatol. 37 https://doi.org/10.1029/2021PA004309.
Edwards, C.T., 2019. Links between early Paleozoic oxygenation and the Great Ordovician Biodiversification Event (GOBE): A review. Palaeoworld 28, 37–50. https://doi.org/10.1016/j.palwor.2018.08.006.
Edwards, C.T., Saltzman, M.R., Leslie, S.A., Bergström, S.M., Sedlacek, A.R.C., Howard, A., Bauer, J.A., Sweet, W.C., Young, S.A., 2015. Strontium isotope (87Sr/86Sr) stratigraphy of Ordovician bulk carbonate: Implications for preservation of primary seawater values. Bull. Geol. Soc. Am. 127, 1275–1289. https://doi.org/10.1130/B31149.1.
Edwards, C.T., Saltzman, M.R., Royer, D.L., Fike, D.A., 2017. Oxygenation as a driver of the Great Ordovician Biodiversification Event. Nat. Geosci. 10, 925–929. https://doi.org/10.1038/s41561-017-0006-3.
Edwards, C.T., Fike, D.A., Saltzman, M.R., Lu, W., Lu, Z., 2018. Evidence for local and global redox conditions at an early Ordovician (Tremadocian) mass extinction. Earth Planet. Sci. Lett. 481, 125–135. https://doi.org/10.1016/j.epsl.2017.10.002.
Edwards, C.T., Fike, D.A., Saltzman, M.R., 2019. Testing carbonate-associated sulfate (CAS) extraction methods for sulfur isotope stratigraphy: A case study of a Lower–Middle Ordovician carbonate succession, Shingle Pass, Nevada, USA. Chem. Geol. 529, 119297 https://doi.org/10.1016/j.chemgeo.2019.119297.
Edwards, C.T., Jones, C.M., Quinton, P.C., Fike, D.A., 2022. Oxygen isotope ($\delta^{18}O$) trends measured from Ordovician conodont apatite using secondary ion mass spectrometry (SIMS): Implications for paleo-thermometry studies. Bull. Geol. Soc. Am. 134, 261–274. https://doi.org/10.1130/B35891.1.
Elmqvist, T., Folke, C., Nyström, M., Peterson, G., Bengtsson, J., Walker, B., Norberg, J., 2003. Response diversity, ecosystem change, and resilience. Front. Ecol. Environ. 1, 488–494. https://doi.org/10.1890/1540-9295(2003)001[0488:RDECAR]2.0.CO;2.
Erickson, B.E., Helz, G.R., 2000. Molybdenum(VI) speciation in sulfidic waters: Stability and lability of thiomolybdates. Geochim. Cosmochim. Acta 64, 1149–1158. https://doi.org/10.1016/S0016-7037(99)00423-8.
Fan, H., Nielsen, S.G., Owens, J.D., Auro, M., Shu, Y., Hardisty, D.S., Horner, T.J., Bowman, C.N., Young, S.A., Wen, H., 2020. Constraining oceanic oxygenation during the Shuram excursion in South China using thallium isotopes. Geobiology 18, 348–365. https://doi.org/10.1111/gbi.12379.
Fike, D.A., Grotzinger, J.P., Pratt, L.M., Summons, R.E., 2006. Oxidation of the Ediacaran Ocean. Nature 444, 744–747. https://doi.org/10.1038/nature05345.
Fike, D.A., Bradley, A.S., Rose, C.V., 2015. Rethinking the ancient sulfur cycle. Annu. Rev. Earth Planet. Sci. 43, 593–622. https://doi.org/10.1146/annurev-earth-060313-054802.
Froelich, P.N., Klinkhammer, G.P., Bender, M.L., Luedtke, N.A., Heath, G.R., Cullen, D., Dauphin, P., Hammond, D., Hartman, B., Maynard, V., 1979. Early oxidation of organic matter in pelagic sediments of the eastern equatorial Atlantic: suboxic diagenesis. Geochim. Cosmochim. Acta 43, 1075–1090. https://doi.org/10.1016/0016-7037(79)90095-4.
Goldberg, S.L., Present, T.M., Finnegan, S., Bergmann, K.D., 2021. A high-resolution record of early Paleozoic climate. In: Proceedings of the National Academy of Sciences, vol. 118. https://doi.org/10.1073/pnas.2013083118.
Goldman, D., Sadler, P.M., Leslie, S.A., Melchin, M.J., Agterberg, F.P., Gradstein, F.M., 2020. The Ordovician Period. In: Geologic Time Scale, 2020, pp. 631–694. https://doi.org/10.1016/B978-0-12-824360-2.00020-6.
Gomes, M.L., Hurtgen, M.T., 2015. Sulfur isotope fractionation in modern euxinic systems: Implications for paleoenvironmental reconstructions of paired sulfate-sulfide isotope records. Geochim. Cosmochim. Acta 157, 39–55. https://doi.org/10.1016/j.gca.2015.02.031.
Hammarlund, E.U., Dahl, T.W., Harper, D.A.T., Bond, D.P.G., Nielsen, A.T., Bjerrum, C.J., Schovsbo, N.H., Schönlaub, H.P., Zalasiewicz, J.A., Canfield, D.E., 2012. A sulfidic driver for the end-Ordovician mass extinction. Earth Planet. Sci. Lett. 331–332, 128–139. https://doi.org/10.1016/j.epsl.2012.02.024.
Haq, B.U., Schutter, S.R., 2008. A chronology of Paleozoic sea-level changes. Science 322, 64–68. https://doi.org/10.1126/science.1161648.
Hardisty, D.S., et al., 2018. An evaluation of sedimentary molybdenum and iron as proxies for pore fluid paleoredox conditions. Am. J. Sci. 318, 527–556. https://doi.org/10.2475/05.2018.04.
Harper, D.A.T., 2006. The Ordovician biodiversification: setting an agenda for marine life. Palaeogeogr. Palaeoclimatol. Palaeoecol. 232, 148–166. https://doi.org/10.1016/j.palaeo.2005.07.010.
Harper, D.A.T., Hammarlund, E.U., Rasmussen, C.M.Ø., 2014. End Ordovician extinctions: A coincidence of causes. Gondwana Res. 25, 1294–1307. https://doi.org/10.1016/j.gr.2012.12.021.
Hayes, J.M., Strauss, H., Kaufman, A.J., 1999. The abundance of ^{13}C in marine organic matter and isotopic fractionation in the global biogeochemical cycle of carbon during the past 800 Ma. Chem. Geol. 161, 103–125. https://doi.org/10.1016/S0009-2541(99)00083-2.
Hetzel, A., Böttcher, M.E., Wortmann, U.G., Brumsack, H.J., 2009. Paleo-redox conditions during OAE 2 reflected in Demerara rise sediment geochemistry (ODP Leg 207). Palaeogeogr. Palaeoclimatol. Palaeoecol. 273, 302–328. https://doi.org/10.1016/j.palaeo.2008.11.005.
Horita, J., Zimmermann, H., Holland, H.D., 2002. Chemical evolution of seawater during the Phanerozoic: Implications from the record of marine evaporites. Geochim. Cosmochim. Acta 66, 3733–3756. https://doi.org/10.1016/S0016-7037(01)00884-5.
Ibach, L.E.J., 1982. Relationship between Sedimentation Rate and Total Organic Carbon Content in Ancient Marine Sediments. AAPG Bull. 66 https://doi.org/10.1306/03B59A5D-16D1-11D7-8645000102C1865D.
Kah, L.C., Thompson, C.K., Henderson, M.A., Zhan, R., 2016. Behavior of marine sulfur in the Ordovician. Palaeogeogr. Palaeoclimatol. Palaeoecol. 458, 133–153. https://doi.org/10.1016/j.palaeo.2015.12.028.
Kendall, B., et al., 2015. Uranium and molybdenum isotope evidence for an episode of widespread ocean oxygenation during the late Ediacaran Period. Geochim. Cosmochim. Acta 156, 173–193. https://doi.org/10.1016/j.gca.2015.02.025.
Kozik, N.P., Young, S.A., Bowman, C.N., Saltzman, M.R., Them, T.R., 2019. Middle–Upper Ordovician (Darriwilian–Sandbian) paired carbon and sulfur isotope stratigraphy from the Appalachian Basin, USA: Implications for dynamic redox conditions spanning the peak of the Great Ordovician Biodiversification Event.

Palaeogeogr. Palaeoclimatol. Palaeoecol. 520, 188–202. https://doi.org/10.1016/j.palaeo.2019.01.032.
Kozik, N.P., Gill, B.C., Owens, J.D., Lyons, T.W., Young, S.A., 2022. Geochemical Records Reveal Protracted and Differential Marine Redox Change Associated with late Ordovician climate and Mass Extinctions. AGU Adv. 3, 1–17. https://doi.org/10.1029/2021av000563.
Kozik, N.P., Young, S.A., Lindskog, A., Ahlberg, P., Owens, J.D., 2023. Protracted oxygenation across the Cambrian–Ordovician transition: a key initiator of the Great Ordovician Biodiversification Event? Geobiology 1–18. https://doi.org/10.1111/gbi.12545.
Krause, A.J., Mills, B.J.W., Zhang, S., Planavsky, N.J., Lenton, T.M., Poulton, S.W., 2018. Stepwise oxygenation of the Paleozoic atmosphere. Nat. Commun. 9, 1–10. https://doi.org/10.1038/s41467-018-06383-y.
Kröger, B., Franeck, F., Rasmussen, C.M.Ø., 2019. The evolutionary dynamics of the early Palaeozoic marine biodiversity accumulation. Proc. R. Soc. B Biol. Sci. 286, 3–8. https://doi.org/10.1098/rspb.2019.1634.
Lang, X., Tang, W., Ma, H., Shen, B., 2020. Local environmental variation obscures the interpretation of pyrite sulfur isotope records. Earth Planet. Sci. Lett. 533, 1–7. https://doi.org/10.1016/j.epsl.2019.116056.
Lau, K.V., Romaniello, S.J., Zhang, F., 2019. The Uranium Isotope Paleoredox Proxy: Moss Landing Marine, pp. 1–30. https://doi.org/10.1017/9781108584142.
Lenton, T.M., Dahl, T.W., Daines, S.J., Mills, B.J.W., Ozaki, K., Saltzman, M.R., Porada, P., 2016. Earliest land plants created modern levels of atmospheric oxygen. Proc. Natl. Acad. Sci. U. S. A. 113, 9704–9709. https://doi.org/10.1073/pnas.1604787113.
Lenton, T.M., Daines, S.J., Mills, B.J.W., 2018. COPSE reloaded: an improved model of biogeochemical cycling over Phanerozoic time. Earth Sci. Rev. 178, 1–28. https://doi.org/10.1016/j.earscirev.2017.12.004.
Lindskog, A., Eriksson, M.E., 2017. Megascopic processes reflected in the microscopic realm: sedimentary and biotic dynamics of the Middle Ordovician "orthoceratite limestone" at Kinnekulle, Sweden. Gff 139, 163–183. https://doi.org/10.1080/11035897.2017.1291538.
Macdonald, F.A., Swanson-Hysell, N.L., Park, Y., Lisiecki, L., Jagoutz, O., 2019. Arc-continent collisions in the tropics set Earth's climate state. Science 364, 181–184. https://doi.org/10.1126/science.aav5300.
Maletz, J., Ahlberg, P., 2011. The :erhamn drill core and its bearing for the graptolite biostratigraphy of the Ordovician Tøyen Shale in Scania, Southern Sweden. Lethaia 44, 350–368. https://doi.org/10.1111/j.1502-3931.2010.00246.x.
Maletz, J., Ahlberg, P., 2021. Dapingian to lower Darriwilian (Middle Ordovician) graptolite biostratigraphy and correlation of the Krapperup drill core, Scania, Sweden. Gff 143, 16–39. https://doi.org/10.1080/11035897.2020.1822439.
Maletz, J., Ahlberg, P., Lundberg, F., 2020. Ordovician graptolite biostratigraphy of the Röstånga-2 drill core (Scania, southern Sweden). Gff 142, 206–222. https://doi.org/10.1080/11035897.2020.1739743.
Maynard, J.B., Force, E.R., 1991. Manganese : Syngenetic deposits on the margins of anoxic basins Chapter 11. Rev. Econ. Geol. 5, 147–157.
McManus, J., Berelson, W.M., Klinkhammer, G.P., Hammond, D.E., Holm, C., 2005. Authigenic uranium: Relationship to oxygen penetration depth and organic carbon rain. Geochim. Cosmochim. Acta 69, 95–108. https://doi.org/10.1016/j.gca.2004.06.023.
Meile, C., Van Cappellen, P., 2003. Global estimates of enhanced solute transport in marine sediments. Limnol. Oceanogr. 48, 777–786. https://doi.org/10.4319/lo.2003.48.2.0777.
Meyers, P.A., 1994. Preservation of elemental and isotopic source identification of sedimentary organic matter. Chem. Geol. 114, 289–302. https://doi.org/10.1016/0009-2541(94)90059-0.
Miller, K.G., Kominz, M.A., Browning, J.V., Wright, J.D., Mountain, G.S., Katz, M.E., Sugarman, P.J., Cramer, B.S., Christie-Blick, N., Pekar, S.F., 2005. The Phanerozoic record of global sea-level change. Science 310, 1293–1298. https://doi.org/10.1126/science.1116412.
Neretin, L.N., Volkov, I.I., Böttcher, M.E., Grinenko, V.A., 2001. A sulfur budget for the Black Sea anoxic zone. Deep-Sea Res. Part I: Oceanogr. Res. Pap. 48, 2569–2593. https://doi.org/10.1016/S0967-0637(01)00030-9.
Newby, S.M., Owens, J.D., Schoepfer, S.D., Algeo, T.J., 2021. Transient Ocean oxygenation at end-Permian mass extinction onset shown by thallium isotopes. Nat. Geosci. 14, 678–683. https://doi.org/10.1038/s41561-021-00802-4.
Nielsen, S.G., Rehkämper, M., Porcelli, D., Andersson, P., Halliday, A.N., Swarzenski, P. W., Latkoczy, C., Günther, D., 2005. Thallium isotope composition of the upper continental crust and rivers - an investigation of the continental sources of dissolved marine thallium. Geochim. Cosmochim. Acta 69, 2007–2019. https://doi.org/10.1016/j.gca.2004.10.025.
Nielsen, S.G., Williams, H.M., Griffin, W.L., O'Reilly, S.Y., Pearson, N., Viljoen, F., 2009. Thallium isotopes as a potential tracer for the origin of cratonic eclogites. Geochim. Cosmochim. Acta 73, 7387–7398. https://doi.org/10.1016/j.gca.2009.09.001.
Nielsen, S.G., Goff, M., Hesselbo, S.P., Jenkyns, H.C., LaRowe, D.E., Lee, C.T.A., 2011. Thallium isotopes in early diagenetic pyrite - a paleoredox proxy? Geochim. Cosmochim. Acta 75, 6690–6704. https://doi.org/10.1016/j.gca.2011.07.047.
Ostrander, C.M., Owens, J.D., Nielsen, S.G., 2017. Constraining the rate of oceanic deoxygenation leading up to a cretaceous Oceanic Anoxic Event (OAE-2: ~94 Ma). Sci. Adv. 3, 1–6. https://doi.org/10.1126/sciadv.1701020.
Ostrander, C.M., Nielsen, S.G., Owens, J.D., Kendall, B., Gordon, G.W., Romaniello, S.J., Anbar, A.D., 2019. Fully oxygenated water columns over continental shelves before the Great Oxidation Event. Nat. Geosci. 12, 186–191. https://doi.org/10.1038/s41561-019-0309-7.
Ostrander, C.M., et al., 2020. Thallium isotope ratios in shales from South China and northwestern Canada suggest widespread O_2 accumulation in marine bottom waters was an uncommon occurrence during the Ediacaran Period. Chem. Geol. 557 https://doi.org/10.1016/j.chemgeo.2020.119856.
Owens, J.D., 2019. Application of Thallium Isotopes, vol. 7027. Cambridge University Press. https://doi.org/10.1017/9781108688697.
Owens, J.D., Reinhard, C.T., Rohrssen, M., Love, G.D., Lyons, T.W., 2016. Empirical links between trace metal cycling and marine microbial ecology during a large perturbation to Earth's carbon cycle. Earth Planet. Sci. Lett. 449, 407–417. https://doi.org/10.1016/j.epsl.2016.05.046.
Owens, J.D., Nielsen, S.G., Horner, T.J., Ostrander, C.M., Peterson, L.C., 2017. Thallium-isotopic compositions of euxinic sediments as a proxy for global manganese-oxide burial. Geochim. Cosmochim. Acta 213, 291–307. https://doi.org/10.1016/j.gca.2017.06.041.
Pasquier, V., Bryant, R.N., Fike, D.A., Halevy, I., 2021. Strong local, not global, controls on marine pyrite sulfur isotopes. Sci. Adv. 7, 1–11. https://doi.org/10.1126/sciadv.abb7403.
Pohl, A., Donnadieu, Y., Le Hir, G., Ferreira, D., 2017. The climatic significance of late Ordovician-early Silurian black shales. Paleoceanography 32, 397–423. https://doi.org/10.1002/2016PA003064.
Pohl, A., Ridgwell, A., Stockey, R.G., Thomazo, C., Keane, A., Vennin, E., Scotese, C.R., 2022. Continental configuration controls ocean oxygenation during the Phanerozoic. Nature 608, 523–527. https://doi.org/10.1038/s41586-022-05018-z.
Poulton, S.W., Canfield, D.E., 2005. Development of a sequential extraction procedure for iron: Implications for iron partitioning in continentally derived particulates. Chem. Geol. 214, 209–221. https://doi.org/10.1016/j.chemgeo.2004.09.003.
Raiswell, R., Hardisty, D.S., Lyons, T.W., Canfield, D.E., Owens, J.D., Planavsky, N.J., Poulton, S.W., Reinhard, C.T., 2018. The iron paleoredox proxies: a guide to the pitfalls, problems and proper practice. Am. J. Sci. 318, 491–526. https://doi.org/10.2475/05.2018.03.
Rasmussen, C.M.Ø., Ullmann, C.V., Jakobsen, K.G., Lindskog, A., Hansen, J., Hansen, T., Eriksson, M.E., Dronov, A., Frei, R., Korte, C., Nielsen, A.T., Harper, D.A.T., 2016. Onset of main Phanerozoic marine radiation sparked by emerging Mid Ordovician icehouse. Sci. Rep. 6, 1–9. https://doi.org/10.1038/srep18884.
Rasmussen, C.M.Ø., Kröger, B., Nielsen, M.L., Colmenar, J., 2019. Cascading trend of early Paleozoic marine radiations paused by late Ordovician extinctions. Proc. Natl. Acad. Sci. U. S. A. 116, 7207–7213. https://doi.org/10.1073/pnas.1821123116.
Reinhard, C.T., Planavsky, N.J., Robbins, L.J., Partin, C.A., Gill, B.C., Lalonde, S.V., Bekker, A., Konhauser, K.O., Lyons, T.W., 2013. Proterozoic Ocean redox and biogeochemical stasis. Proc. Natl. Acad. Sci. U. S. A. 110, 5357–5362. https://doi.org/10.1073/pnas.1208622110.
Rue, E.L., Smith, G.J., Cutter, G.A., Bruland, K.W., 1997. The response of trace element redox couples to suboxic conditions in the water column: Deep-Sea Research Part I. Oceanogr. Res. Pap. 44, 113–134. https://doi.org/10.1016/S0967-0637(96)00088-X.
Sahoo, S.K., Planavsky, N.J., Jiang, G., Kendall, B., Owens, J.D., Wang, X., Shi, X., Anbar, A.D., Lyons, T.W., 2016. Oceanic oxygenation events in the anoxic Ediacaran Ocean. Geobiology 14, 457–468. https://doi.org/10.1111/gbi.12182.
Saltzman, M.R., Edwards, C.T., Leslie, S.A., Dwyer, G.S., Bauer, J.A., Repetski, J.E., Harris, A.G., Bergström, S.M., 2014. Calibration of a conodont apatite-based Ordovician 87Sr/86Sr curve to biostratigraphy and geochronology: Implications for stratigraphic resolution. Bull. Geol. Soc. Am. 126, 1551–1568. https://doi.org/10.1130/B31038.1.
Sampaio, E., Santos, C., Rosa, I.C., Ferreira, V., Pörtner, H.O., Duarte, C.M., Levin, L.A., Rosa, R., 2021. Impacts of hypoxic events surpass those of future ocean warming and acidification. Nat. Ecol. Evol. 5, 311–321. https://doi.org/10.1038/s41559-020-01370-3.
Scotese, C., 2001. Atlas of earth history, Vol 1: Paleogeography. PALEOMAP Proj. http://scotese.com.
Scott, C., Lyons, T.W., 2012. Contrasting molybdenum cycling and isotopic properties in euxinic versus non-euxinic sediments and sedimentary rocks: refining the paleoproxies. Chem. Geol. 324–325, 19–27. https://doi.org/10.1016/j.chemgeo.2012.05.012.
Scott, C., Lyons, T.W., Bekker, A., Shen, Y., Poulton, S.W., Chu, X., Anbar, A.D., 2008. Tracing the stepwise oxygenation of the Proterozoic Ocean. Nature 452, 456–459. https://doi.org/10.1038/nature06811.
Sepkoski, J.J., Bambach, R.K., Raup, D.M., Valentine, J.M., 1981. Phanerozoic marine diversity and the fossil record. Nature 293, 435–437. https://doi.org/10.1038/293435a0.
Servais, T., Owen, A.W., Harper, D.A.T., Kröger, B., Munnecke, A., 2010. The Great Ordovician Biodiversification Event (GOBE): the palaeoecological dimension. Palaeogeogr. Palaeoclimatol. Palaeoecol. 294, 99–119. https://doi.org/10.1016/j.palaeo.2010.05.031.
Servais, T., Cascales-Minana, B., Harper, D.A.T., 2021. The Great Ordovician Biodiversification Event (GOBE) is not a single event. Paleontol. Res. 25, 315–328. https://doi.org/10.2517/2021PR001.
Sperling, E.A., Wolock, C.J., Morgan, A.S., Gill, B.C., Kunzmann, M., Halverson, G.P., Macdonald, F.A., Knoll, A.H., Johnston, D.T., 2015. Statistical analysis of iron geochemical data suggests limited late Proterozoic oxygenation. Nature 523, 451–454. https://doi.org/10.1038/nature14589.
Sperling, E.A., et al., 2021. A long-term record of early to mid-Paleozoic marine redox change. Sci. Adv. 7 https://doi.org/10.1126/sciadv.abf4382.
Stigall, A.L., Edwards, C.T., Freeman, R.L., Rasmussen, C.M.Ø., 2019. Coordinated biotic and abiotic change during the Great Ordovician Biodiversification Event: Darriwilian assembly of early Paleozoic building blocks. Palaeogeogr. Palaeoclimatol. Palaeoecol. 530, 249–270. https://doi.org/10.1016/j.palaeo.2019.05.034.
Taylor, S.R., McLennan, S.M., 1981. The composition and evolution of the continental crust: rare earth element evidence from sedimentary rocks. Philos. Trans. R. Soc.

Lond. Ser. A Math. Phys. Sci. 301, 381–399. https://doi.org/10.1098/rsta.1981.0119.
Taylor, S.R., McLennan, S.M., 1995. The geochemical the continental evolution crust. Rev. Mineral. Geochem. 33, 241–265.
Them, T.R., Gill, B.C., Caruthers, A.H., Gerhardt, A.M., Gröcke, D.R., Lyons, T.W., Marroquín, S.M., Nielsen, S.G., João, P.T.A., Owens, J.D., 2018. Thallium isotopes reveal protracted anoxia during the Toarcian (early Jurassic) associated with volcanism, carbon burial, and mass extinction. Proc. Natl. Acad. Sci. U. S. A. 115, 6596–6601. https://doi.org/10.1073/pnas.1803478115.
Thompson, C.K., Kah, L.C., 2012. Sulfur isotope evidence for widespread euxinia and a fluctuating oxycline in early to Middle Ordovician greenhouse oceans. Palaeogeogr. Palaeoclimatol. Palaeoecol. 313–314, 189–214. https://doi.org/10.1016/j.palaeo.2011.10.020.
Thullner, M., Dale, A.W., Regnier, P., 2009. Global-scale quantification of mineralization pathways in marine sediments: a reaction-transport modeling approach. Geochem. Geophys. Geosyst. 10 https://doi.org/10.1029/2009GC002484.
Torsvik, T.H., et al., 2012. Phanerozoic Polar Wander, Palaeogeography and Dynamics. Earth-Science Reviews 114, 325–368. https://doi.org/10.1016/j.earscirev.2012.06.007.
Tribovillard, N., Algeo, T.J., Lyons, T., Riboulleau, A., 2006. Trace metals as paleoredox and paleoproductivity proxies: an update. Chem. Geol. 232, 12–32. https://doi.org/10.1016/j.chemgeo.2006.02.012.
Tribovillard, N., Bout-Roumazeilles, V., Algeo, T., Lyons, T.W., Sionneau, T., Montero-Serrano, J.C., Riboulleau, A., Baudin, F., 2008. Paleodepositional conditions in the Orca Basin as inferred from organic matter and trace metal contents. Mar. Geol. 254, 62–72. https://doi.org/10.1016/j.margeo.2008.04.016.
Trotter, J.A., Williams, I.S., Barnes, C.R., Lecuyer, C., Nicoll, R.S., 2008. Did Cooling Oceans Trigger Ordovician Biodiversification? Evidence from Conodont Thermometry. Science 321, 550–554. https://doi.org/10.1126/science.1155814.
Uramoto, G.I., et al., 2019. Significant contribution of subseafloor microparticles to the global manganese budget. Nat. Commun. 10, 1–10. https://doi.org/10.1038/s41467-019-08347-2.
Young, S.A., Saltzman, M.R., Foland, K.A., Linder, J.S., Kump, L.R., 2009. A major drop in seawater 87Sr/86Sr during the Middle Ordovician (Darriwilian): Links to volcanism and climate? Geology 37, 951–954. https://doi.org/10.1130/G30152A.1.
Young, S.A., Gill, B.C., Edwards, C.T., Saltzman, M.R., Leslie, S.A., 2016. Middle–Late Ordovician (Darriwilian–Sandbian) decoupling of global sulfur and carbon cycles: Isotopic evidence from eastern and southern Laurentia. Palaeogeogr. Palaeoclimatol. Palaeoecol. 458, 118–132. https://doi.org/10.1016/j.palaeo.2015.09.040.
Young, S.A., Benayoun, E., Kozik, N.P., Hints, O., Martma, T., Bergström, S.M., Owens, J. D., 2020. Marine redox variability from Baltica during extinction events in the latest Ordovician–early Silurian. Palaeogeogr. Palaeoclimatol. Palaeoecol. 554, 109792 https://doi.org/10.1016/j.palaeo.2020.109792.
Zhang, J., Li, C., Fang, X., Li, W., Deng, Y., Tu, C., Algeo, T.J., Lyons, T.W., Zhang, Y., 2022. Progressive expansion of seafloor anoxia in the Middle to late Ordovician Yangtze Sea: Implications for concurrent decline of invertebrate diversity. Earth Planet. Sci. Lett. 598, 117858 https://doi.org/10.1016/j.epsl.2022.117858.